Impact of ocean acidification (OA) on the acid-base regulation of polar cod: Time and localized tracking of brain pH changes

Masterarbeit

zur Erlangung des Grades eines

Master of Science (M.Sc.)

Universität Rostock

Mathematisch-

Naturwissenschaftliche Fakultät

Prof. Dr. Inna Sokolova

In Kooperation mit dem Alfred-

Wegener-Institut für Polar- und

Meeresforschung, Bremerhaven

Dr. Christian Bock

Universität Rostock Traditio et Innovatio

ALFRED-WEGENER-INSTITUT HELMHOLTZ-ZENTRUM FÜR POLAR- UND MEERESFORSCHUNG

Vorgelegt von Clara Isabella Scheuring

September 2019

Table of Content

List of figures

List of tables

Abbreviations

ANOVA	Analysis of variance
AO	Arctic ocean
aq	Aqueous
ATP	Adenosinetriphosphate
B. saida	*Boreogadus saida*
BS	Barents Sea
BSA	Bovine serum albumin
C	Cerebellum
$CaCO_3$	Calcium Carbonate
cAMP	Cyclic Adenosine monophosphate
CC	Cerebellar crest of the rhombencephalon
CCb	Corpus division of the cerebellum
CEST	Chemical exchange saturation transfer
Cl^-	Chloride

cm	Centimetre
CO_2	Carbon dioxide
CO_3^{2-}	Carbonate
^{13}C	Carbon isotope with mass number 13
D	Diencephalon
δ	Chemical shift
DIC	Dissolved inorganic carbon
DMO	5,5-dimethyl-2,4-oxazolidinedione
DOM	Dissolved organic matter
EG	Eminentia granularis
ENS	European Nordic seas
Eq	Equivalent
fig	Figure
FISP	Fast imaging with steady state precession
FOV	Field of view
g	Grams
GABA	Gamma amino butyric acid
$GABA_AR$	Gamma aminobutyric acid type A receptor
GHG	Greenhouse gas
Gt	Giga tons
h	Hour(s)
HCO_3^-	Hydrogen carbonate
ht	Header tanks
H_2O	Water
^1H	Hydrogen isotope with mass number 1
IPCC	Intergovernmental Penal on Climate Change
K^+	Potassium
KCl	Potassium chloride
KH_2PO_4	Potassium dihydrogen phosphate
LS	Laptev Sea

M	Mesencephalon
mm	Millimeter
mM	Millimolar
mmHg	Millimetre of mercury
MO	Medulla oblongata
MRI	Magnetic resonance imaging
MRT	Magnetic resonance tomograph
ms	Milliseconds
NaCl	Sodium chloride
Na_2HPO_4 * $2H_2O$	Disodium hydrogen phosphate dihydrate
NMR	Nuclear magnetic resonance
OA	Ocean acidification
olt	Olfactory tract
P	Pons
PBS	Phosphate buffered saline
PCr	Phosphocreatine
pCO_2	Partial pressure of CO_2
Pd	Phosphodiester
pH	$-\log10[H^+]$
pH_e	Extracellular pH
pH_i	Intracellular pH
pH_w	Water pH
Pi	Inorganic phosphate
ppm	Parts per million
^{31}P	Phosphorous isotope with mass number 31
RARE	Rapid acquisition with relaxation enhancement
RF	Radio frequency
ROI	Region of interest
ru	Relative units

SC	Spinal cord
sP	Sugar phosphate
SRES	Special report on emission scenarios
T	Tesla
TA	Total alkalinity
TauCEST	Chemical exchange saturation transfer from taurine to water
T_E	Echo time
Tec	Tectum
Tel	Telencephalon
TO	Optic Tectum
T_R	Repetition time
TMAO	Trimethylamine *N*-oxide
W	Watt
Ø	Diameter
%	Percent

Zusammenfassung

Durch Kohlenstoffdioxid (CO_2), das sich in der Atmosphäre akkumuliert, verändert sich unser Klima, was zum globalen Klimawandel führt. Das CO_2 löst sich zudem im Ozean, wo es den pH-Wert des Wassers reduziert und zu einer Ozeanversauerung (OA) führt. Lange wurde davon ausgegangen, dass Fische von dieser Versauerung nicht betroffen wären, da sie über eine effektive Säure-Base Regulation verfügen. In den letzten Jahren wiesen jedoch verschiedene Studien darauf hin, dass eine Reduktion des pH-Werts Verhaltensänderungen und Veränderungen in neurologischen Prozessen herbeiführen kann. Um die Säure-Base Regulation im Gehirn des Polardorschs (*Boreogadus saida*) zu untersuchen, wurden in dieser Studie zwei Methoden, die auf dem Phänomen der Nuklearen Magnetischen Resonanz (NMR) beruhen, kombiniert. Mit nicht-lokalisierter ^{31}P-NMR Spektroskopie konnte die Konzentration verschiedener Phosphormetabolite bestimmt werden. Mithilfe von ^{31}P-NMR Spektroskopie können kurzzeitige Änderungen der Konzentrationen der Phosphormetabolite und damit kurzzeitige Änderungen des intrazellulären pH (pH_i) bestimmt werden. Der pH_i wurde aus der chemischen Verschiebung des Signals von anorganischem Phosphat zu Phosphorkreatin bestimmt. Da nicht-lokalisierte ^{31}P-NMR Spektroskopie allerdings nicht den pH in einem Areal von der Größe eines Fischhirns bestimmen kann, sollten über den Sättigungstransfer einer chemischen Verschiebung (chemical exchange saturation transfer (CEST)) ortsaufgelöst pH-Änderungen verfolgt werden. CEST ist eine Bildgebungsmethode, die den Austausch zwischen den Protonen des Wassers mit austauschbaren Protonen von Metaboliten detektiert, wie zum Beispiel Taurin (TauCEST) im Gehirn von *B. saida*. Der CEST Effekt ist unter anderem pH abhängig und kann somit Änderungen im pH_i ortsaufgelöst über das Gehirn aufzeigen. Zusätzlich zu pH Änderungen wurde der Energiestoffwechsel von *B. saida* unter akuter Versauerung mittels ^{31}P-NMR Spektroskopie analysiert. ^{31}P-NMR Spektroskopie misst die Konzentration von anorganischem Phosphat, Phosphorkreatin und den drei ATP Untereinheiten α-, β- und γ-ATP. Nach 20 Stunden Akklimatisierung unter Kontrollbedingungen wurden die Fische für vier Stunden einer CO_2 Konzentration von 3500 ppm (Hyperkapnie) und einem Wasser pH von 6.92 ± 0.2 ausgesetzt. Danach wurden die Fische wieder unter Kontrollbedingungen untersucht (pH 7.96 ± 0.3). Nach Umschalten auf Hyperkapnie sank der pH_i im Mittel um 0.5 ± 0.2 pH-Einheiten. Bei zwei Fischen lag die maximale Reduktion des pH_i bei 0.17 pH-Einheiten. Signifikante Veränderungen im Energiestoffwechsel konnte bei keinem Tier festgestellt werden.

Abstract

A consequence of accumulating carbon dioxide (CO_2) in the atmosphere is global climate change. CO_2 also dissolves in the ocean and reduces the water pH, resulting in ocean acidification (OA). Fish were long thought to be relatively resistant to pH changes in the water, because they possess an efficient acid-base regulation. However, recent findings indicate altered behaviour and changes in neurological processes in fish. To investigate the acid-base regulation in the brain of the polar cod (*Boreogadus saida*), a combination of two methods, based on the nuclear magnetic resonance (NMR) phenomenon, was used in this study. Non-localized ^{31}P-NMR spectroscopy was used to measure the concentration of phosphometabolites. The intracellular pH (pH_i) was calculated from the chemical shift of the NMR signal of inorganic phosphate in relation to the phosphocreatine signal. ^{31}P-NMR spectroscopy is used to detect short-term changes in the concentration of different phosphometabolites and hence short-term changes in the pH. However, the determination of the pH value in a specific region as small as the fish brain is not possible with non-localized ^{31}P-NMR spectroscopy. To verify the results of the measurements the chemical exchange saturation transfer (CEST) between taurine and water (TauCEST) was determined in a specific region in the brain of *B. saida*. Because CEST is pH dependant, changes in the CEST effect can give evidence on any pH changes with a higher spatial resolution than non-localized ^{31}P-NMR spectroscopy. Additionally to pH changes, energy metabolism can be analysed with ^{31}P-NMR spectroscopy by measuring the concentration of phosphometabolites such as inorganic phosphate, phosphocreatine or the three ATP subunits α-, β- and γ-ATP. After 20 hours of acclimatisation under control conditions, the animals were exposed to a CO_2 concentration of 3500 ppm and a water pH of 6.92 ± 0.2 for four hours (hypercapnia). Then, the animals were tested again in water without elevated CO_2 concentrations (pH 7.96 ± 0.3). The pH_i decreased rapidly after switching to hypercapnia by a mean of 0.05 ± 0.2 and started to reach control values again after two hours. The maximum decrease in pH_i was 0.17 and occurred in fish 2 and 4. Throughout the whole time of the experiment, there were no significant changes in the energy values.

1 Introduction

1.1 Climate change in the Arctic ocean

The ocean plays a major role in regulating the Earth's climate, since it absorbs over 25% of the atmospheric carbon dioxide (CO_2) and 90% of the heat that accumulates in the atmosphere (Gattuso 2015). Through anthropogenic effects and the Industrial Revolution, atmospheric partial pressure of CO_2 (pCO_2) rose from 280 ppm before the Industrial Revolution to a maximum of 413.9 ppm in 2019, leading to a global climate change (Bijma & Burhop 2010, https://www.co2.earth/daily-co2). Atmospheric CO_2 levels are predicted to rise to 750 – 1000 ppm by the end of the century (Pörtner 2008, Meinshausen et al. 2011). Three major stressors are associated with climate change: warming, deoxygenation and acidification, all affecting marine ecosystems and their productivity (Bopp et al. 2013, Popova et al. 2016). As temperature in the oceans rises, marine ecosystems suffer from many negative impacts, including mass mortality of marine invertebrates due to heat stress, shifts in the distribution of marine species and associated structural changes in marine communities (Oliver et al. 2017, 2018). Rising temperature in Arctic environments leads to melting sea ice, posing a problem for many marine organisms, who depend on the sea ice (Chambault et al. 2018). Temperature strongly affects exothermic organisms, including fish (Boscolo-Galazzo et al. 2018).

Another aspect of global climate change is ocean deoxygenation (Gómez1 et al. 2018, Junium et al. 2018). Global warming decreases the solubility of gases in the seawater leading to less dissolved oxygen in the open ocean (Gilbert & Rabalais 2010, Popova et al. 2016). With oxygen levels below 2 $ml l^{-1}$ the ecosystem is defined as hypoxic (Diaz & Rosenberg 1995). Benthic organisms evolved tolerance mechanisms to hypoxia, but fish are more sensitive to decreasing oxygen concentrations and mass mortality has been reported (Diaz & Rosenberg 1995).

Besides ocean warming and expanding hypoxia, global climate change leads to another problem, referred to as ocean acidification (OA) (Caldeira & Wickett 2003, Melzner et al. 2009, Bozinovic & Pörtner 2015). The atmospheric CO_2 dissolves in the ocean and when it dissociates, hydrogen ions are being released (according to the following formula), which results in a lower pH (Orr et al. 2005, Bijma & Burhop 2010).

$$CO_2 + H_2O \leftrightarrow H_2CO_3 \leftrightarrow H^+ + HCO_3^- \leftrightarrow 2H^+ + CO_3^{2-} \quad [1]$$

The current pH in the seawater surface is around 8.05, but by absorbing the atmospheric CO_2, the pH of the seawater decreases as it has already by 0.1 units compared to pre-industrial times

(Orr et al. 2005, Gruber et al. 2012, Wermter et al. 2018). Moreover, it is expected to decrease up to 0.77 units by 2300 due to global climate change (Caldeira & Wickett 2003, Heuer & Grosell 2018).

To which extent global climate change will affect these processes depends on emission scenarios (Caldeira &Wickett 2005). There are six different scenarios of future CO_2 emissions, as well as other greenhouse gas emissions estimated by the intergovernmental panel on climate change (IPCC). Three scenarios belong to the A1 storyline and estimate very rapid economic growth, a peak in global population development in the mid-century and are distinguished by different technologies used in the energy system. The A2 storyline describes a continuously increasing global population, slower changes in technologies and primarily regional economic development. This scenario shows the highest long-term greenhouse gas emissions and is the one closest to reality at the moment (IPCC 2014). The technology changes in the B2 scenario are more diverse and sustainable than in all the other scenarios. Global population growth is also continuously increasing but not as fast as in the A2 scenario (IPCC 2000). The least long-term greenhouse gas emissions are estimated in the B1 scenario that

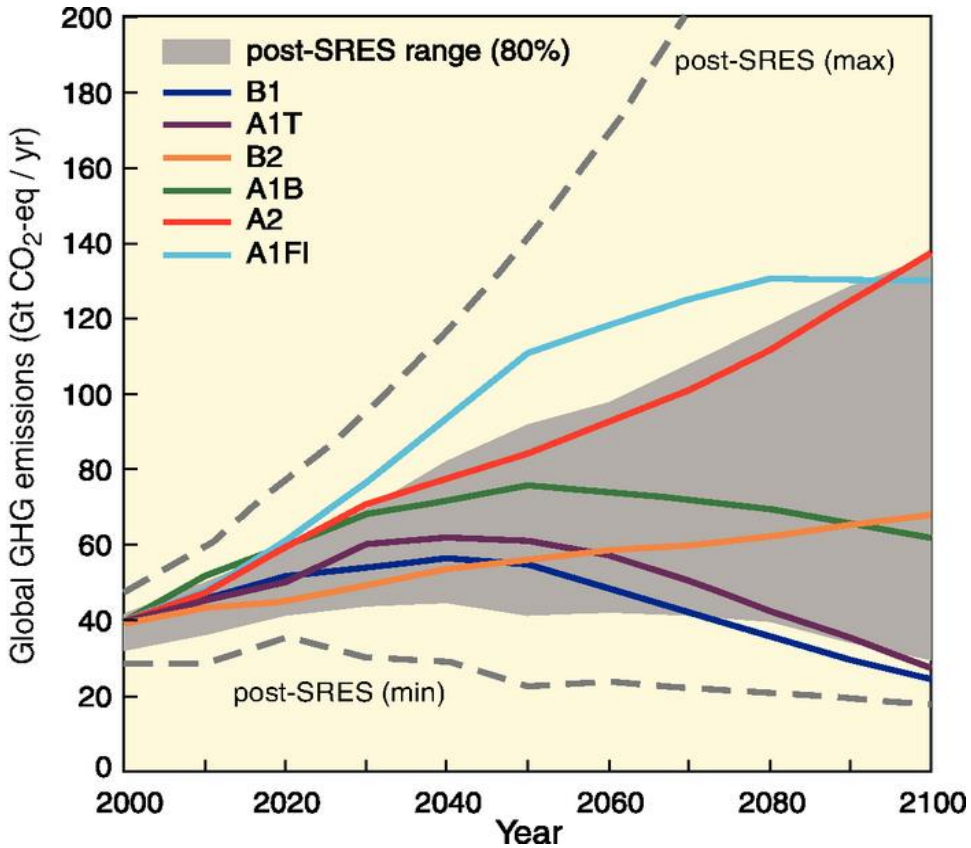

Figure 1: Global Greenhouse gas (GHG) emissions (in $GtCO_2$-equivalent per year) in the absence of additional climate policies: the special report on emission scenarios (SRES) A1B, A1Fl, A1T, A2, B1 and B2 (coloured lines) and 80th percentile range of recent scenarios published since SRES (post-SRES) (grey shaded area). Dashed lines show the full range of post-SRES scenarios. The GHG emissions include CO_2, CH_4, N_2O and F-gases. www.ipcc.ch AR4 Report

describes a rapid change in energy technologies towards clean and sustainable methods and the same population growth as described in the A1 scenario. All six emission rate scenarios are illustrated in figure 1. Estimated changes in the future ocean pH at the Bay of California according to the high-emission A2 scenario are shown in figure 2 by Gruber et al. (2012). Biastoch et al. (2014) predict a pH decrease of 0.25 units in the Arctic ocean within the next 100 years. Not only does the ocean pH decrease with rising CO_2 concentrations in the atmosphere, but also the concentrations of carbonate (CO_3^{2-}) in the ocean decreases as

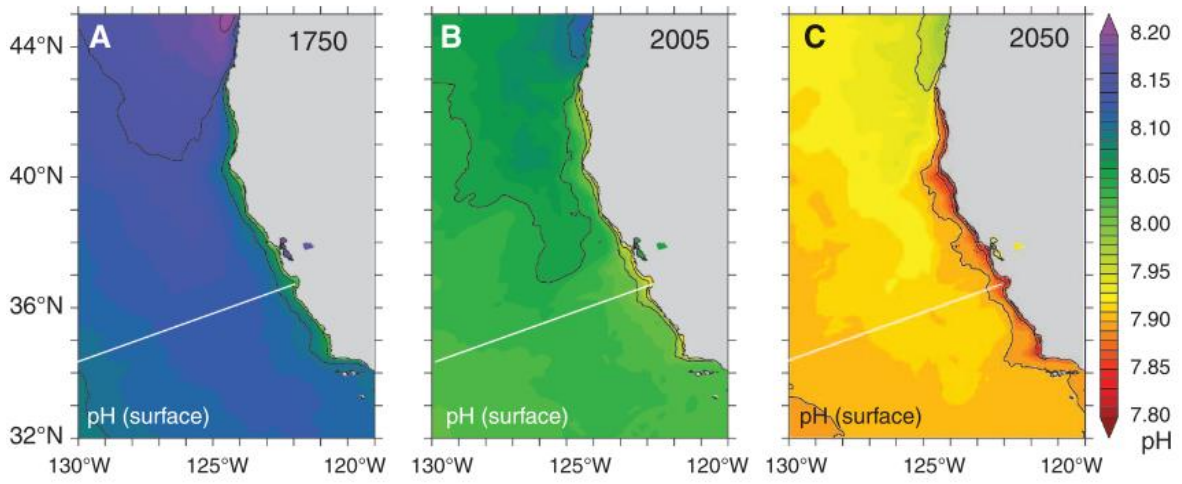

Figure 2: Evolution of the water pH off the coast of California from 1750 until 2050. C shows the predicted decrease in ocean pH for the A2 IPCC scenario (Gruber et al. 2012).

CO_2[aq] increases, according to formula 1 (Orr et al. 2005, Kroeker et al. 2013). This makes it difficult for marine calcifying organisms like corals or bivalves to form biogenic calcium carbonate ($CaCO_3$), which results in deformed shells or lowered calcification rates (Kroeker et al. 2013, Liu et al. 2018). Therefore, many studies have been done on the effects of OA on calcifying organisms (Orr et al. 2005, Kroeker et al. 2013, Boch et al. 2018, Zittier et al. 2018).

Temperature and pH changes occur faster in polar regions than in other environments (Field et al. 2018, Zittier et al. 2018). As seen in figure 4, the mean bottom water temperature in the Barents Sea is between 2 - 5°C (Fall et al. 2018, Petrini et al. 2018). It has already increased by about 3°C compared to 1985, whereas the global average temperature has only increased by 1°C (Hassol 2004). It is predicted that Arctic sea surface temperatures will rise by about three times the global average (Praetorius et al. 2018). This so called Arctic amplification is a result of weather events like clouds, surface albedo and poleward oceanic and atmospheric heat transport (Praetorius et al. 2018). Global warming and ocean acidification affect all marine habitats, but since organisms in the polar oceans are adapted to a narrow temperature range, both processes pose an especially great threat to these habitats and their inhabitants (Kroeker

et al. 2013, Gattuso et al. 2018, Wermter et al. 2018). Moreover, marine populations are projected to move poleward, leading to the occurrence of invasive species in higher latitudes (Turingan & Sloan 2016, Wilson et al. 2016, Monllor-Hurtado et al. 2017).

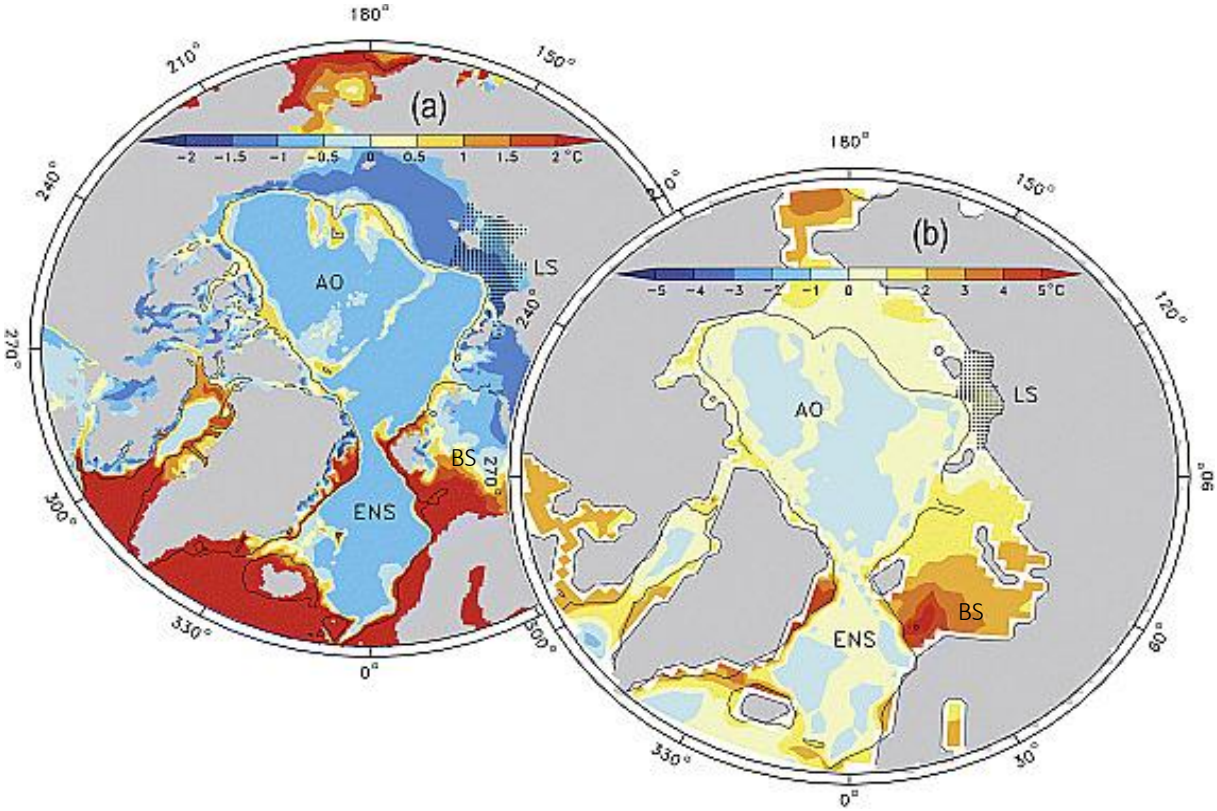

Figure 3: (a) Map of average bottom water temperature between 1985 and 2004 in the arctic ocean and (b) a trend in the next 100 years under CO_2 increase. Acronyms mark the Arctic Ocean (AO), European Nordic Seas (ENS), Barents Sea (BS) and the Laptev Sea (LS) (Biastoch et al. 2014).

1.2 Polar cod, *Boreogadus saida*

The polar cod (*Boreogadus saida;* Lepechin, 1774 (fig. 5)), a pelagic, schooling fish, one of the most abundant fish species in the Arctic and subarctic waters, is an important polar organism, because it links several trophic levels (Welch et al. 1992). It reaches a size of up to 46 cm (see Hop & Gjøsæter 2013 for review) while the mean size is 30 cm with a weight of 33 g (Scott & Scott 1988, Welch et al. 1992). The maximum age is found to be seven years, but rarely exceeds the age of five (Bradstreet et al. 1986, Hop et al. 1997, Ajiad et al. 2011). Schools of adult polar cods have been found under the sea ice as well as in the open water during summer (Crawford & Jorgenson 1990, Hop et al. 1997). The polar cod feeds on copepods living directly under the sea ice surface and hence lives in close association with the sea ice (Lønne & Gulliksen 1989). The polar cod itself is an important prey for seabirds and marine mammals, such as the white whale (*Delphinapterus leucas,* Pallas, 1776), the narwhal (*Monodon monoceros,* Linnaeus, 1758) and the ringed seal (*Pusa hispida*, Schreber, 1775) because of its high lipid/energy

content (Welch et al. 1992, Kühn et al. 2018, Landry et al. 2018). Therefore, *B. saida* is responsible for a major part of the energy transfer from primary and secondary production to higher trophic levels in the arctic ecosystem (Welch et al. 1992, Hop & Gjøsæter 2013). *B. saida* lives in water temperatures that range from -2°C in winter up to 8°C in summer (Drost et al. 2014). However, its temperature preference has been determined experimentally to be at 3 – 4°C (Christiansen et al. 1996). The distribution in water temperature below the thermal optimum is most likely due to reduced competition as well as special adaptations (Hop & Gjøsæter 2013). As part of the arctic ecosystem *B. saida* is adjusted to constant low temperatures and as an example has antifreeze glycoproteins (Zhuang et al. 2012). Cattano et al. (2018) discovered that pelagic species, like *B. saida*, are more likely to die from high CO_2 levels than benthic species. This may be due to more stable CO_2 concentrations in the open ocean, whereas at the ocean bottom CO_2-levels naturally fluctuate (Hofmann et al. 2011, Munday et al. 2011, Murray et al. 2014). Therefore, it is crucial to investigate any effects of OA and global warming on *B. saida* to gain knowledge and make predictions on the whole Arctic ecosystem concerning global warming (Kühn et al. 2018, Landry et al. 2018).

Figure 4:A picture of Boreogadus saida *taken by Hauke Flores*

1.3 Polar fish in a changing environment

Temperature is a driver in species distribution and population structures (Pörtner et al. 2008). Rising temperatures are predicted to shift species distributions towards the poles (Perry et al. 2005). With climate change the distribution and abundance of *B. saida* is declining in the Barents Sea, whereas its boreal relative, the Atlantic cod (*Gadus morhua,* Linnaeus, 1758), shifted its distribution poleward (Decamps et al. 2017). Diet content is considered to differ between the two species hence no evidence for prey competition was found (Renaud et al. 2012). However, a possible predation of *G. morhua* on *B. saida* has been suggested (Renaud et al. 2012). A major impact climate change has on the Arctic ecosystem, namely *B. saida,* is the decreasing sea ice. Since spawning for *B. saida* is reported during winter under the sea ice, this

threatens its reproduction (Craig et al. 1982). Kunz et al. (2016) investigated different parameters such as growth rate and thermal optimum for both *B. saida* and *G. morhua* under climate change conditions. Their findings suggest a slower growth rate of 0.39% d^{-1} for *B. saida* than for *G. morhua*, which showed a growth rate of 0.82% d^{-1}. *G. morhua* also showed a higher tolerance to projected future pCO_2 values than *B. saida* (Kunz et al. 2016).

The current temperature trend goes hand in hand with a decreasing ocean pH and OA (Pörtner et al. 2004). Additionally, OA also results in a reduction of the surface water oxygen level, which may affect the degree of sensitivity of an organism to other environmental factors (Pörtner et al. 2005). Organisms living in an environment with elevated CO_2 levels have elevated energy costs (Ishimatsu et al. 2008). However, costs for energy-dependent metabolic processes can be minimalised by specialising on a narrow temperature range as appearing in polar regions (Pörtner 2006). During acute respiratory acidosis from OA, reductions in extracellular blood pH (pH_e) and intracellular pH (pH_i) have been observed (Pörtner et al. 2005, Shartau et al. 2016). Influences on the energy budget affect physiology, development and behaviour (Nilsson et al. 2012, Heuer & Grosell 2016, 2018).

1.4 pH regulation in fish

Fish were long thought not to be as sensitive to elevated CO_2 levels and pH changes as marine invertebrates, because of their effective acid-base regulation and the higher regulatory capacity of ion exchange (Claiborne et al. 2002, Melzner et al. 2009, Pörtner et al. 2011, Cattano et al. 2018). As well as controlling their pH_i through active ion transport, fish have epithelia which limit ion losses, because ions can only pass the membrane through specific channels (Pörtner et al. 2005). However, they react to elevated CO_2 partial pressure (pCO_2) (hypercapnia) by increasing their ventilation rate (Pörtner et al. 2005), reducing protein synthesis (Langenbuch & Pörtner 2017), behavioural disturbances (Schmidt 2019), metabolic depression (Pörtner et al. 2004) and eventually cardiac failure (Ishimatsu et al. 2004). Even higher mortality was discovered in fish that have been exposed to long term elevated CO_2 concentration, but the exact reasons remain unknown (Ishimatsu et al. 2008). When the intracellular pH drops, fish excrete H^+ ions across the gills, kidney and intestine as a countermeasure (Ishimatsu et al. 2008, Heisler 1986). The gill epithelium is the first regulatory site, therefore being the main epithelium for acid-base transfer to the water (Claiborne et al. 2002). The pH homeostasis in the brain is provided by transporting or buffering of acid equivalents (Sinning & Hübner 2013).

With acid-base relevant ions like chloride (Cl^-) or bicarbonate (HCO_3^-), fish regulate and maintain their tissue pH (Chung et al. 2014). However, during hypercapnia the CO_2 equilibrium is shifted, according to formula 1, towards HCO_3^- and H^+ (Shartau et al. 2016). This equilibrium shift lowers the internal pH and results in acidosis (Shartau et al. 2016). Previous studies showed that a decreasing pH in the brain leads to a decrease in the rate of synaptic vesicle release which ultimately results in a limited excitability of the brain (Sinning & Hübner 2013, Wermter et al. 2018). Brain pH changes indicate neurological as well as behavioural disorders through disturbances in the acid-base balance of the organism (Wermter et al. 2018, Schmidt 2019). The gamma-aminobutyric acid type A receptor ($GABA_AR$) is a Cl^- and HCO_3^- channel, activated by the neurotransmitter GABA (gamma amino butyric acid) (see for instance Schmidt et al. 2018). After GABA binding, the channel allows Cl^- and HCO_3^- to pass the cell membrane, resulting in a hyperpolarization and causing less neuronal activity (Chung et al. 2014). Therefore, a decreasing pH leads to a decreasing neuronal activity, whereas an increasing pH leads to an increasing neuronal activity (Sinning & Hübner 2013). During high CO_2 exposure the membrane gradients of Cl^- and HCO_3^-, and therefore, the $GABA_AR$ function, is disturbed (Chung et al. 2014). This disturbance leads to a slower reaction of the animal (Chung et al. 2014). In addition to this, Chivers et al. (2014) found that fish cannot process sensory information during CO_2 exposure. This matches the results of Ferrari et al. (2012), suggesting that the visual system is affected by high CO_2 concentrations. Therefore, pH_i regulation in the brain is very important. When exposed to CO_2 and then treated with the $GABA_AR$ blocker gabazine, the effects of CO_2 can be neutralized as shown in figure 5 (Nilsson et al. 2012, Chung et al. 2014, Munday et al. 2016).

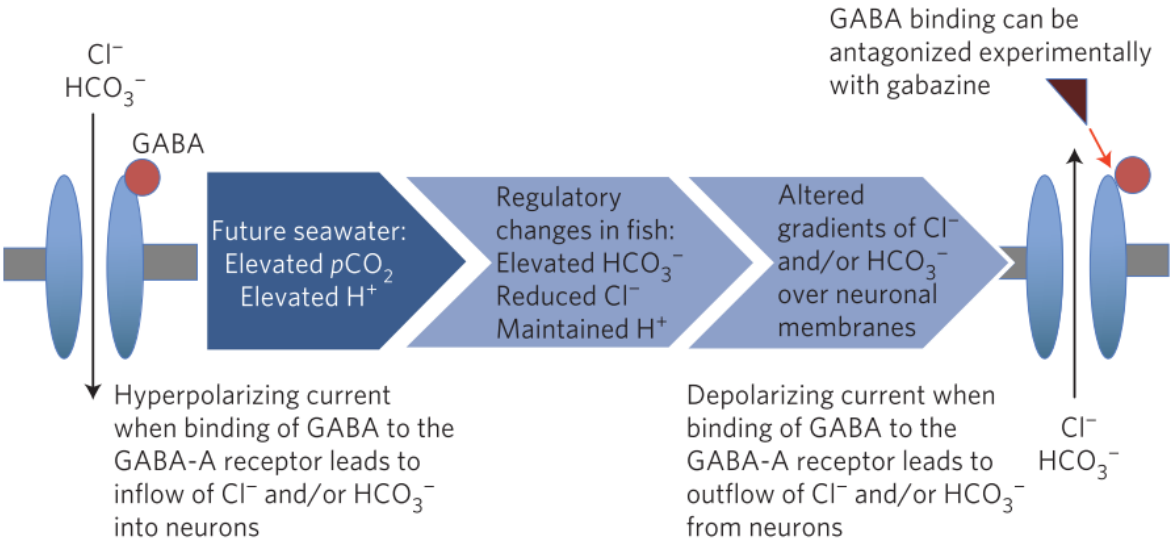

Figure 5: Model of the $GABA_AR$ to show hypercapnia-induced changes published by Nilsson et al. 2012. Normally functioning $GABA_AR$ (left) leading to a hyperpolarisation of the cell by an Cl^-/HCO_3^- inflow after GABA binding. A $GABA_AR$ in a gabazine treatment (right) leading to a depolarisation of the cell by a Cl^-/HCO_3^- outflow.

1.5 Magnetic resonance imaging (MRI) and NMR spectroscopy

Magnetic resonance imaging (MRI) and nuclear magnetic resonance (NMR) spectroscopy can give insight into the neurological processes in the brain of an animal (Schmidt et al. 2014). These techniques are non-invasive and do not use harmful radiation, but radio frequency (RF) and are, therefore, a useful method for repeatedly gaining information about the intact, living organism (Lee et al. 2010). Metabolism and stress responses can be followed directly in various tissues (Van den Thillart et al. 1989, Lee et al. 2010). Both techniques are based on the physical phenomenon of NMR (Bloch 1946, Purcell et al. 1946). An object in the magnetic resonance tomograph (MRT) is exposed to a very strong magnetic field leading, to a polarisation of the nuclei (Schild 1990). This polarisation is referred to as longitudinal magnetisation along the external magnetic field (Schild 1990). The nuclei commonly used for MRI and MRS are either protons (^1H) or other nuclei, such as phosphorous (^{31}P) or carbon (^{13}C) (Lee et al. 2010, Pritchard & Flemming Hansen 2019). Then, the RF is applied and absorbed by the nuclei, causing the nuclei to point in one direction, the transverse direction (Schild 1990). The RF decreases longitudinal magnetisation and builds up transversal magnetisation (Schild 1990). Depending on the choice of nuclei, the RF needs to be adjusted, because different nuclei absorb different RF (Schild 1990). When the RF is switched off, the system returns to its relaxed state and resonance frequency is emitted during this relaxation (Schild 1990). Nuclei in different tissues vary in relaxation time which leads to different contrasts in the MRI (Schild 1990). NMR spectroscopy determines the chemical shift that occurs when the nucleus emits modulated

resonance frequency in a changed chemical surrounding (Lee et al. 2010). The obtained spectrum provides information about the concentration of different metabolites in a chosen tissue (Lee et al. 2010). ^{31}P-NMR spectroscopy can be used to investigate acid-base regulation as well as energy metabolism (Van der Linden et al. 2004). However, alongside the mentioned applications in energy metabolism and acid-base regulation, there is a variety of applications for NMR technologies. After establishing a clinical method of MRI of the head, also cardiac imaging was possible to evaluate cardiovascular disease (Hawkes et al. 1981, Herfkens et al. 1983) as well as three-dimensional anatomical images (Matthaei et al. 1986). MRI is a useful method for identifying different regions in a tissue or organ (Van der Linden et al. 2004, Miraux et al. 2008). Different regions of the brain of *B. saida* have been recorded from the MRI scans and identified after Ou & Yamamoto (2016) who worked on *Trachurus japonicus* (Temminck & Schlegel, 1844). An anatomical drawing of *T. japonicus* is shown in figure 6 (Ou & Yamamoto 2016). Anatomical MR images of *B. saida* in a coronal, sagittal and axial plane are displayed in figure 7 with a description of different regions in the brain.

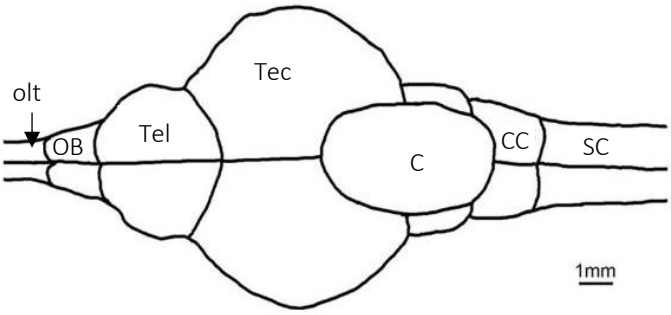

Figure 6: Technical drawing of the brain of B. saida *with the olfactory tract (olt), olfactory bulb (OB), telencephalon (Tel), optic tectum (Tec), Cerebellum (C), cerebellar crest of the rhombencephalon (CC) and spinal cord (SC). Identification of the brain regions according to Ou & Yamamoto 2016 and Kawaguchi et al. 2019*

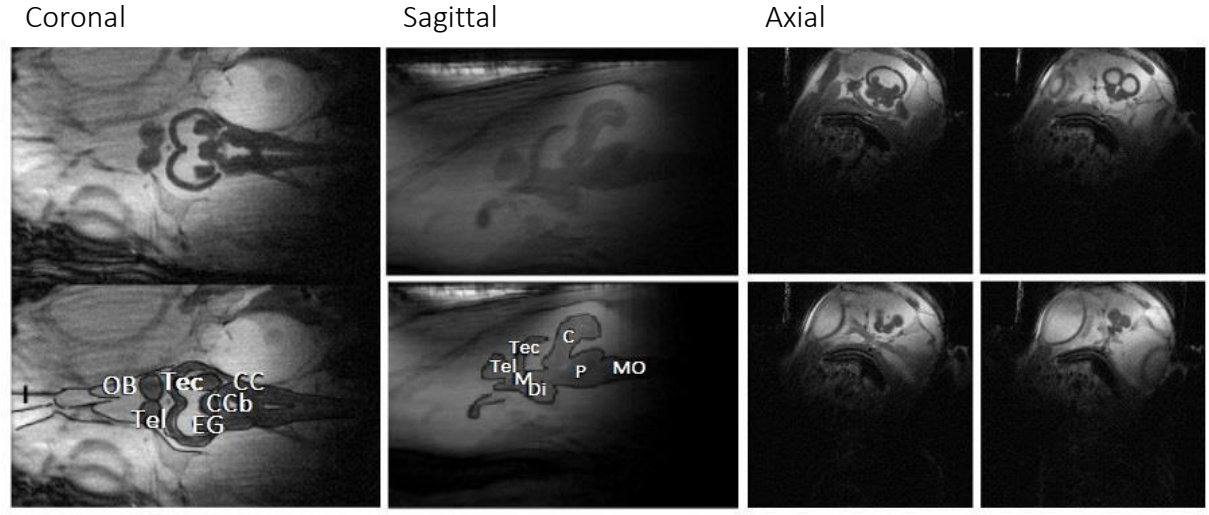

Figure 7: Brain regions of polar cod on MRI scans with OB, Tec, Tel, C, CC, eminentia granularis (EG), Corpus division of the Cerebellum (CCb), Mesencephalon (M), Diencephalon (Di), Pons (P) and Medula oblongata (MO)

Performing MR technology on marine animals is especially challenging (Van der Linden et al. 2004, Lee et al. 2010). Working with aquatic animals is challenging alone but seawater implies even more obstacles due to the high salt concentration. The animal inside the MRT needs a constant flow of aerated water (Van der Linden et al. 2004). But water motion can lead to artefacts in the MRI and it is crucial that the water does not come in contact with the gradient (Van der Linden et al. 2004). Therefore, different ways have been developed to overcome these obstacles. To guarantee a constant water flow without flooding the MRT, a metal free chamber can be used to place the fish inside the MRT, connected to water pools outside the MRT. Different RF antenna have been evolved which can be placed in the water free space outside the chamber on top of the measured region (Van der Linden et al. 2004).

1.6 Chemical exchange saturation transfer

Recently, Ward et al. (2000) introduced a MRI technique that uses the exchange of protons (^{1}H) as a contrast agent. This technique is called chemical exchange saturation transfer (CEST). Its principle is illustrated in figure 8. Exchangeable protons get excited by a set frequency and thereby selectively saturated which reduces magnetisation, ultimately leading to zero magnetisation. The saturated protons of the solute then exchange with the unsaturated protons in the tissue water with a defined exchange rate. The saturated protons accumulate in the tissue water leading to a reduced signal intensity of the water proportional to the solute concentration (Kogan et al. 2013). While the saturation frequency is applied and water magnetisation decreases, longitudinal relaxation brings the saturated protons back to their thermal equilibrium state (Kogan et al. 2013). The chemical shift between both resonance frequencies of the water and the solute protons is then measured in parts per million (ppm). The CEST effect is displayed in

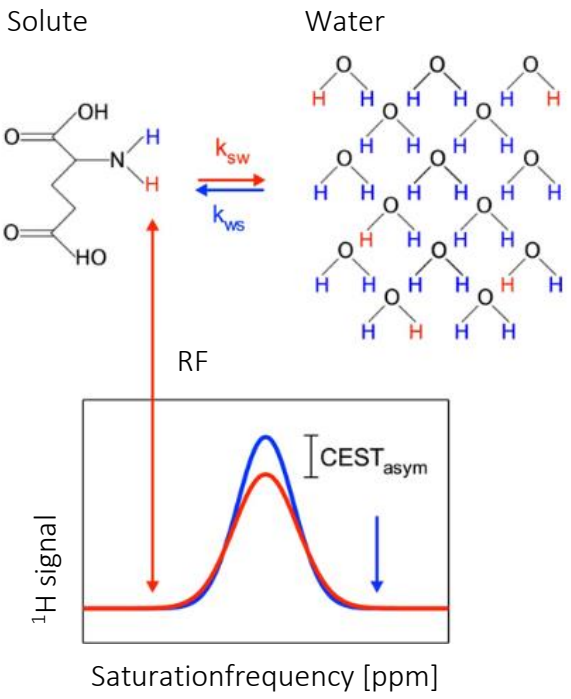

Figure 8: The principle of CEST is illustrated above. Protons of a solute being saturated by a specific RF. Saturated protons of the solute then exchange with water protons, thereby decreasing the water signal proportional to the solute concentration. Modified illustration by Wermter (2017)

the form of the z-spectrum (fig. 15) by plotting the water signal as a function of the saturation frequency and given in percent depending on the amount of exchanging protons (Kogan et al. 2013). The intensity of the CEST effect is pH and temperature dependant (Ward & Balaban 2000, Wermter et al. 2018)

CEST was tested with many different amino acids, such as alanine, glutamine or taurine as well as other solutes (Walker-Samuel et al. 2017). Taurine is important for neuronal activity and osmoregulation (Ripps & Shen 2012). Due to its osmoregulatory function, taurine is one of the most abundant amino acids in the brain of marine vertebrates and therefore easily detectable by the CEST application performed at low temperatures (Ripps & Shen 2012, Wermter et al. 2018). With the chemical exchange saturation transfer from taurine to water (TauCEST), it is possible to detect changes in the acid-base regulation of ectothermic animals, especially those living in a cold environment, like *B. saida* (Wermter et al. 2018). Wermter et al. (2018) were the first to investigate the TauCEST effect on the brain of the polar cod at high CO_2 levels. The chemical shift between the amine protons of taurine and the water protons is assumed to be 2.8 ppm (Wermter et al. 2018). TauCEST is a non-invasive, *in vivo* method to detect even small changes in the pH under high CO_2 exposure with high resolution (Wermter et al. 2018). By using ^{1}H-NMR spectroscopy Wermter et al. (2018) could proof that the TauCEST in the brain of *B. saida* was not due to changes in the taurine concentration. In contrast to other *in vivo* methods this method gives the opportunity to see anatomical images of an unanaesthetised and ventilating fish, without the need for dissection (Wermter et al. 2018).

1.7 Hypotheses

The aim of this study will be to investigate pH_i changes in the brain of *B. saida* caused by rising CO_2 concentrations in the seawater. As previously mentioned, the polar cod is an important organism in Arctic waters as it links different trophic levels. Thus, it is of major interest to study its ecology and physiology in respect to a changing pH_i as a result of OA.

Most studies that investigated the effects on pH_i changes in the brain of marine animals so far have either been invasive, *in vitro* or they haven't been conducted on polar fish species (Mark et al. 2002, Munday et al. 2011, Murray et al. 2014, Wermter et al. 2018). In order to investigate these changes, a combination of pH_i determination with ^{31}P-NMR spectroscopy and CEST will be applied and the following hypotheses are going to be tested:

- Hypercapnia induced acid-base regulation starts right after *B. saida* is exposed to environmental acidification and helps the cell to maintain pH_i in hypercapnic conditions.
- *B. saida* is able to compensate the hypercapnia induced decrease in pH_i over time
- pH_i decreases during hypercapnia by up to 0.2 pH units
- The drop in pH_e leads to metabolic depression in *B. saida*, effecting the cellular energy demand.

2 Material and Methods

2.1 Collection of the experimental animals

The animals used in this study were caught on the research vessel Heincke during the cruise HE 519 in October 2018. The animals were collected in a depth of 130 - 190 m, in a temperature of -1 - -1.5 °C in the Billefjord of Svalbard (78°59'N 16°50'E). The animals were captivated in a seawater aquarium at the Alfred-Wegener-Institute, Helmholtz Zentrum für Polar- und Meeresforschung (AWI) in Bremerhaven with a water temperature of 1 °C, a pH of 8 in normocapnia, a salinity of 32 PSU and were fed once a week.

2.2 Experimental setup

For each MR experiment, an individual fish was placed in a Perspex flow-through chamber (V = 350 ml; fig. 9 A). Dental wax was added to the chamber and modulated for each fish individually positioning the fish at the frontal part of the chamber. All animals had enough space to move their fins and gills. Moreover, the seawater circulating system consisted of two heater tanks (ECO RE630, LAUDA GmbH & CO KG, Königshofen, Germany) which kept the water temperature in the chamber at around 0.5°C. Temperature confirmation measurements were performed inside the tanks with a high-precision temperature-measuring instrument (testo 112, testo, Lenzkirch, Germany) and at the outflow of the chamber with a fibre-optical thermometer (OPTOCON

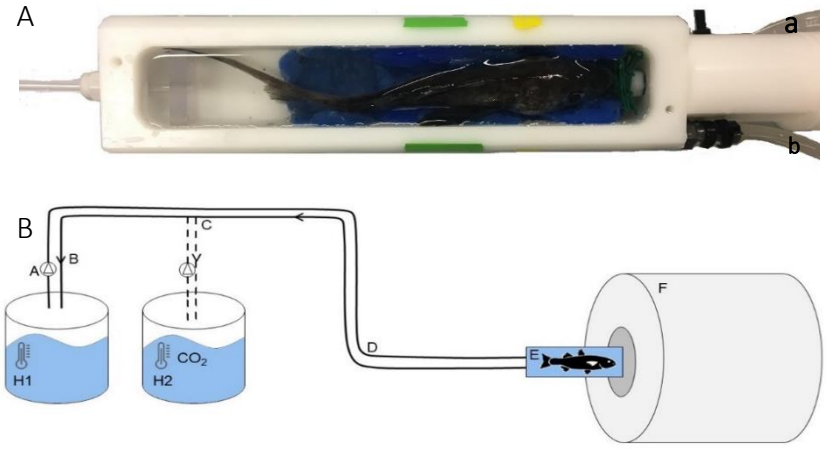

Figure 9: A: Testing chamber with the experimental animal inside and tubes with water inflow (a) and outflow (b). Dental wax helps to position the fish at the frontal part of the chamber. B: Schematic design of the experimental setup with the header tanks H1 (normocapnia) and H2 (hypercapnia), water inflow (A), water outflow (B) in an isolated tube (D), the experimental camber (E) and the MRT (F).

AG, Optical Sensors and Systems, Dresden, Germany). As displayed in figure 9 B each header tank was used for one sea water reservoirs (H1 and H2). H1 with control conditions bubbled with air; and H2 with elevated CO_2 bubbled with an air/CO_2 mixture from a gas-mixing pump (PR 4000, MKS Instruments, Munich, Germany). The water reservoirs were changed once a week.

The pH of the water reservoirs was measured with a conventional pocket meter (pH 3310, WTW, Weilheim, Germany). Water pCO_2 was determined from the gas phase of the sea water by a carbon dioxide sensor filter (CARBOCAP GMP343, Vaisala, Helsinki, Finland). Salinity was measured with a WTW LF 197 multimeter (WTW). Total alkalinity (TA) was measured in an external laboratory (Krisitina Beck, PhD Candidate, Bentho-Pelagic Processes, AWI, Bremerhaven). Since TA was measured only once, no standard deviation (SD) can be given. Dissolved inorganic carbon (DIC) was measured via the continuous flow analysis method with Seal Analysis SFA QuAAtro (AACE 6.07, Seal Analytical, Wisconsin, USA). Bicarbonate $(HCO_3^-)_w$ was calculated via CO2Sys macro for Microsoft Excel (v2.1, Pierrot et al. 2006), with values for K1 and K2 from Millero (2010), KSO4 from Dickson (1990) and $[B]_T$ from Uppström (1974). A summary of water chemistry is given in Table 1. All tests were performed on a 9,4 T NMR-tomograph (BioSpec 94/30 USR, AVANCE III, Bruker BioSpin, Ettlingen, Germany). The *in vivo* ^{31}P-NMR spectra were obtained by using a 2 cm diameter ^{1}H/^{31}P-NMR surface coil. The spectra were plotted and stacked with XWinPlot (Bruker BioSpin MRI GmbH, Ettlingen, Germany). The *in vivo* CEST measurements were performed on a ^{1}H/^{13}C resonator with an inner diameter of 72 mm.

All fish have been placed in the experimental chamber for at least 20 hours to acclimatise before switching to hypercapnia. Three hours prior to the hypercapnic treatment, control measurements were performed, followed by four hours of measurements under hypercapnia. Afterwards, 2 more hours of normocapnia were recorded. The experimental protocol was the same for all *in vivo* MRI and NMR spectroscopy measurements.

All procedures were approved in accordance with the regulations for the welfare of experimental animals issued by the Federal Government of Germany (§11 Abs. Ziff. 1 a+b), Bremen AZ: 0515_2040_15.

Table 1:Seawater chemistry of the control (H1) and the hypercapnic (H2) water reservoirs. Temperature, salinity, pCO_2, pH_w, Total alkalinity and dissolved inorganic carbon were measured and HCO_3^- was calculated via CO2Sys macro for Microsoft excel (v2.1).

Group	T [°C]	S [PSU]	P $(CO_2)_w$ [ppm]	$(HCO_3^-)_w$ [mM]	pH_w	TA [mM]	DIC [mM]
Control	0.3 ± 0.2	30.5 ± 0.4	506 ± 24	1.96	7.96 ± 0.3	2.11	2.13 ± 0.06
Hypercapnia	0.7 ± 0.4	30.5 ± 0.5	3518 ± 110	2.15	6.92 ± 0.2	2.49	2.56 ± 0.1

2.3 *In vivo* ^{31}P-NMR spectroscopy

In vivo ^{31}P-NMR spectroscopy was used to measure energy values and to determine the intracellular pH (pH_i) in the brain of the fish (Lurman et al. 2007, Bock et al. 2008). The spectra were obtained by using a 2 cm diameter ^{1}H-^{31}P-NMR surface coil placed in the water free space outside the Perspex chamber above the head of the animal (fig. 10), to determine the chemical shift (δ) of the inorganic phosphate (Pi) signal relative to the Phosphocreatine (PCr) signal. δ was then used to calculate pH_i by the following formula after Kost (1990) and modified after Bock et al. (2001).

$$pHi = 6.8788 + Log10\frac{(Pi - 2.8) - 0.67 + 0.003579 * 0.5}{(3.2 + 0.001888 * 0.5 - (Pi - 2.8)}$$

PCr was used as an internal standard for spectra calibration and set to 0ppm. Furthermore, the intracellular energy values of tissue can be determined using ^{31}P-NMR spectroscopy by calculating e.g. the ratio of Pi/PCr concentrations. The energy values were calculated as in the following formula.

$$Energy\ values = \frac{Integral\ of\ the\ Pi\ signal}{Integral\ of\ the\ PCr\ signal}$$

Paravison 6.1 Software was used for all NMR measurements. ^{31}P-NMR spectroscopy scans were obtained with a flip angle of 65°, a repetition time T_R = 1200 ms and 256 averages. Acquisition bandwidth was 10 000 Hz and reference power was 2.714 W. All scan properties are given in table 3 in the appendix.

Figure 10: in vivo *MR image of the head of* B. saida *obtained with a $^{1}H/^{13}C$ resonator with an inner diameter of 72 mm. The yellow circle marks the area sensitive to the ^{31}P-NMR-surface coil.*

2.4 CEST measurements

2.4.1 *In vitro* CEST measurements

Before the CEST *in vivo* experiments, a phantom study was performed to investigate the influence of the water parameters pH and temperature as well as the solute concentration of different metabolites found in the fish brain on the CEST effect. The *in vitro* measurements were based on a study by Wermter et al. (2018). The phantoms for the *in vitro* measurements consist of six NMR-tubes (Ø 5 mm) filled with different solutions bedded in a 50 ml Falcon Tube (Fisher Scientific GmbH, Schwerte, Germany) filled with a 3% Agarose solution. The agarose was mixed with deionized water and heated in a microwave until clear. After filling the agarose solution into the Falcon tube, the NMR tubes were inserted (fig. 11). The solutions filled in the NMR-tubes are based on a phosphate buffer. The chemicals were obtained from Sigma Aldrich (St. Louis, USA). A summary of the *in vitro* phantom solutions is given in table 2. All solutions are adjusted to pH values of 6.5; 6.8; 7.0; 7.2, 7.5 and 7.8. All approaches were tested at seven different temperatures between 1 – 37°C.

Figure 11: Phantom tube with different pH values of the same solution in the NMR tubes for the in vitro *CEST study.*

In order to test the phantoms at different temperatures, a water hose (EHEIM GmbH & Co KG, Deizisau, Germany) was wrapped around the Falcon tube, isolated with isolating tape (ArmaFlex, armacell GmbH, Münster, Germany) and connected to a Thermostat (FP30 MH, JULABO GmbH, Seelbach, Germany). The phantom tubes were attached to a positioning aid to push them into the magnet. The object to be tested has to be in the centre of the magnet to get the best possible image.

CEST images were obtained by pre-saturated FISP (fast imaging with steady state precession) scans with a field of view (FOV) 30 x 30 mm^2, a matrix size of 64 x 64, a slice thickness of 2 mm, a flip angle of 9°, a repetition time T_R = 3.2 ms and an echo time T_E = 1.6 ms. Before measuring the CEST effect, B_0

homogeneity was optimized to a line width of 10 Hz or less. Z-spectra were obtained using 50 frequency offsets between −20 000 and 20 000 Hz with respect to the water signal. The experimental design for the *in vitro* study is shown in figure 12. All scan properties are given in table 3 in the appendix.

Table 2: Three different approaches for the in vitro *CEST measurement. One negative control only consisting of PBS. One solution with PBS and BSA [10 mM] and one solution with PBS and TMAO [10mM]. Chemicals with the used concentrations to produce PBS are listed below. All solutions were adjusted to the following pH values: 6.5; 6.8; 7.0; 7.2, 7.5 and 7.8 and tested at seven different temperatures.*

Approach	Solute	Concentration [mM]	Temperature [C°]
Negative control - Phosphate buffered saline (PBS)	NaCl	137.0	1, 5, 10, 15, 20, 25, 37
	KCl	2.7	
	$Na_2HPO_4 * 2H_2O$	10.0	
	KH_2PO_4	1.8	
PBS + Bovine serum albumin (BSA)	PBS		1, 5, 10, 15, 20, 25, 37
	BSA	10	
PBS + Trimethylamine *N*-oxide (TMAO)	PBS		1, 5, 10, 15, 20, 25, 37
	TMAO	10	

Figure 12: Experimental design of the in vitro study with A: header tank; B: water hose; C: isolation; D: NMR tubes with the testing solution; E: magnet resonance tomograph. On the left the realistic proportions are shown.

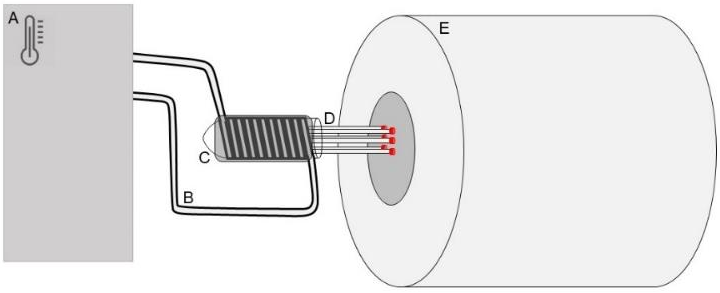

All scan images with different excitation frequencies were stacked to a hyperstack. In every hyperstack the different regions of interest (ROI) in the NMR tubes were selected (fig. 13) and evaluated in Fiji image J (Schindelin et al. 2012, Rueden et al. 2017). The data gained from Fiji

image J was loaded into MATLAB (Version R2019a, The MathWorks Inc., Natick, USA). Z-Spectra (exepmlary shown in fig. 14) were generated in MATLAB.

The CEST effect for a chemical shift at 1 ppm and 2.8 ppm were evaluated (fig. 15). TMAO shows a mean CEST effect for a pH value of 6.5 of 15% ± 20% (15°C) and 27% ± 19% (10°C) as well as a CEST effect of 11% ± 15% for a pH value of 7.5 at 37°C and a chemical shift of 1 ppm. BSA does not show any CEST effect higher than 6% ± 4%, also at a chemical shift of 1 ppm. The CEST effect is much higher for a chemical shift of 1 ppm than for a chemical shift of 2.8 ppm. A graph with a smaller scale for a chemical shift of 2.8 ppm is shown in the appendix

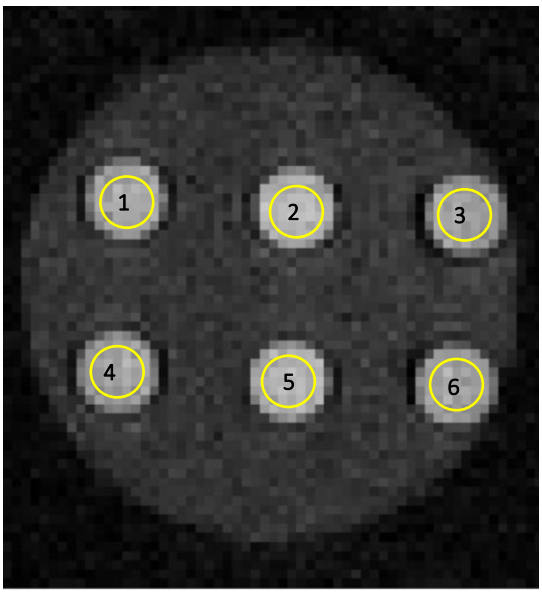

Figure 13:MR image of a phantom with a different pH value (6.5; 6.8; 7.0; 7.2; 7.5; 7.8) in each tube. The yellow circles show the chosen ROI that was evaluated first in Fiji image J and then in MATLAB.

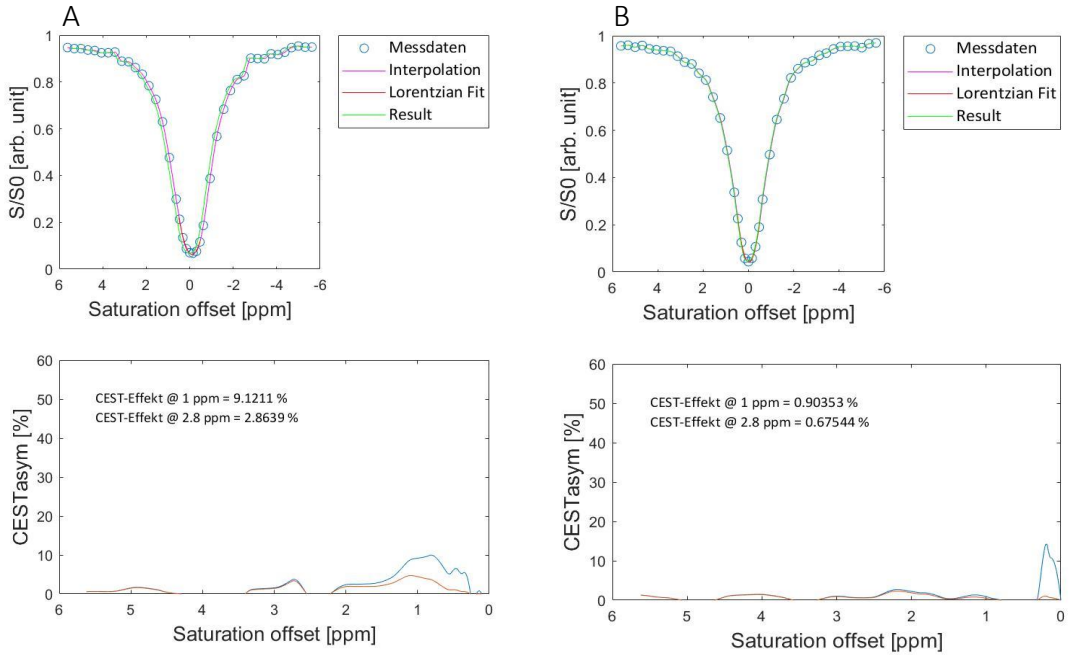

Figure 14: Z-spectra showing the CEST effect in percent for a chemical shift of 1 ppm and 2.8 ppm. In A with a high CEST effect and in B no CEST effect. A shows the CEST effect for TMAO at 15 °C at a pH of 7. B shows the CEST effect for BSA at 5°C at a pH of 7.5.

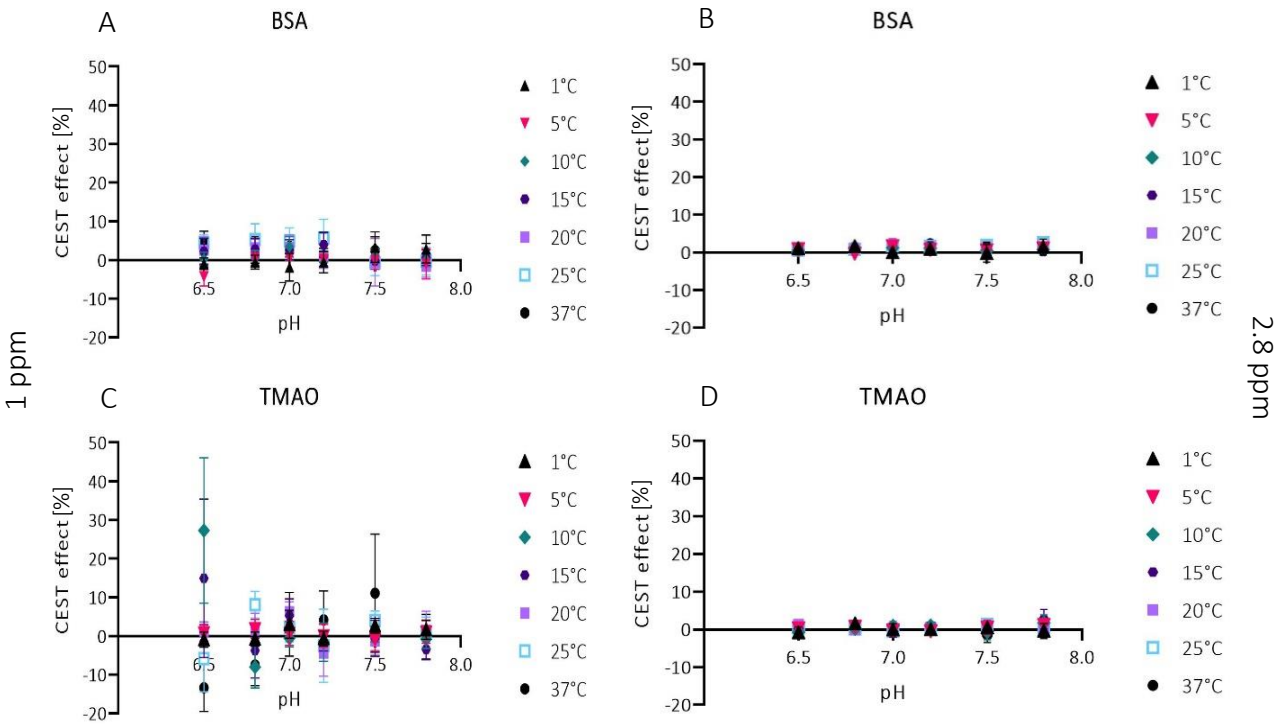

Figure 15: The CEST effect for a chemical shift of 1 ppm in A (BSA) and C (TMAO) and for a chemical shift of 2.8 ppm in B (BSA) and D (TMAO). TMAO shows a CEST effect for δ 1ppm at a pH of 6.5 and a temperature of 10°C and 15°C.

2.4.2 *In vivo* CEST measurements

Pilot and RARE scans (Rapid acquisition with relaxation enhancement) were conducted before the *in vivo* CEST measurements, were performed to detect an optimal slice of the brain. A MRI slice which displays a preferably large area of the brain was chosen for CEST. Measurements were performed in triplets alternating with RARE scans to control the position of the fish. The chosen slice with the ROI is shown in figure 16.

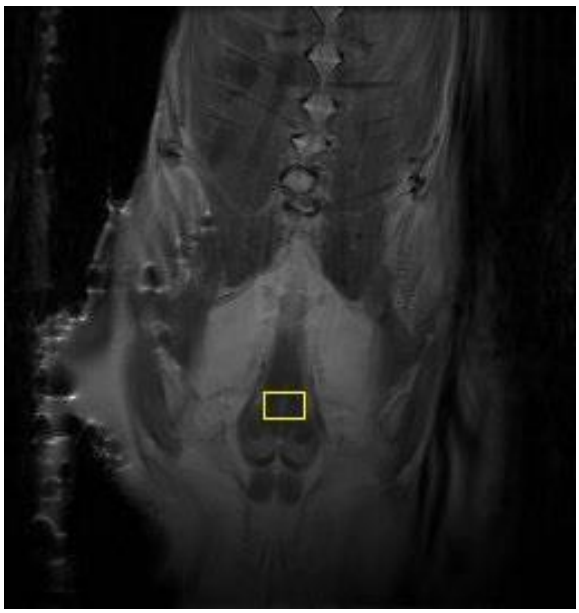

Figure 16: Testing slice for the in vivo *CEST measurements with the chosen ROI in the yellow box. The MRI scan was obtained with a $^{1}H/^{13}C$ resonator with an inner diameter of*

2.5 Statistical analysis

For any significance analysis ANOVA with *post-hoc* tests were performed in GraphPad Prism (Prism Version 8.1.2., GraphPad Software, Inc., San Diego, USA). All graphs were plotted in GraphPad Prism. ANOVA tests were conducted with the pH_i values of three hours before switching to hypercapnia. The pH_i values under hypercapnia as well as the pH_i values under normocapnia were evaluated against the mean of the pH_i values under control conditions.

3 Results

3.1 *In vivo* ^{31}P-NMR spectroscopy

With *in vivo* ^{31}P-NMR spectroscopy it is possible to visualise the abundance and the concentration of phosphometabolites such as sugar phosphates (sP), cyclic adenosinmonophosphate (cAMP), inorganic phosphate (Pi), phosphodiester (Pd), phosphocreatine (PCr) and three different adenosinetriphophate (ATP) subunits α-, β- and γ γ,Figure 17 presents such a spectrum obtained by *in vivo* ^{31}P-NMR spectroscopy under control conditions. All the phosphometabolites mentioned above could be detected. Figure 18 displays the effect of different pH values on the position of Pi and its chemical shift δ to PCr.

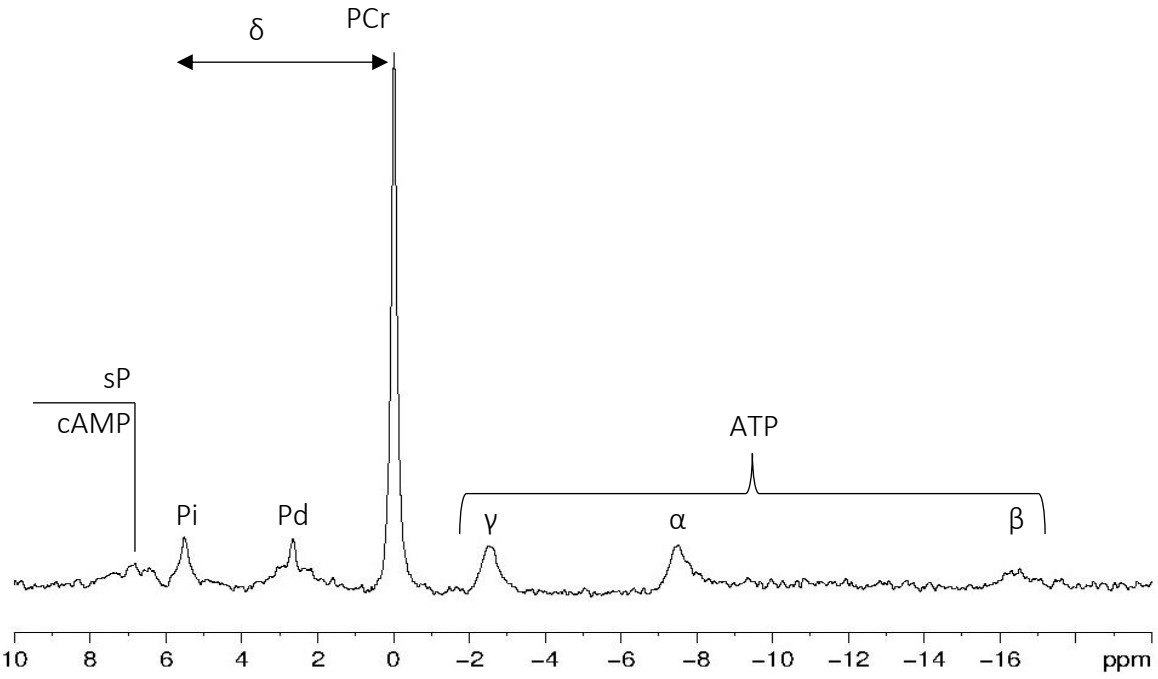

Figure 17: Typical in vivo *^{31}P-NMR spectrum showing relative concentrations of phosphometabolites in a brain cell of* B. saida*. Phosphometabolites in the brain are sP = sugar Phosphates; cAMP = cyclic AMP; Pi = inorganic Phosphate; PCr = Phosphor creatine and the three phosphate groups γ-, α- and ß-ATP. The PCr peak was set to 0 ppm. The other metabolites have a chemical shift in ppm in relation to PCr.*

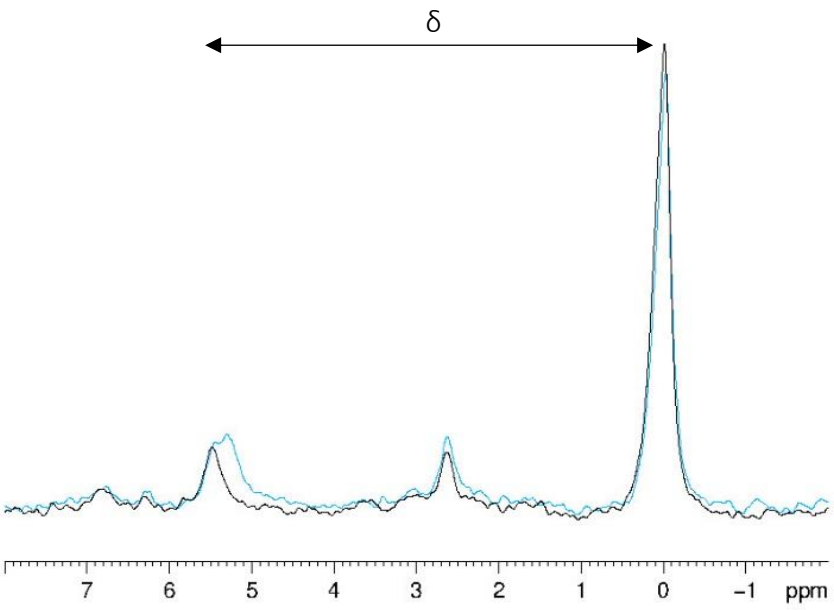

Figure 18: Two ^{31}P-NMR spectra showing a different chemical shift of Pi in relation to PCr. The difference in δ between the two displayed spectra is 0.11 ppm.

Figure 19 A shows a stack plot of *in vivo* ^{31}P-NMR spectra two hours of control conditions prior to hypercapnic conditions. The signal intensity of the ATP signals is relatively stable before switching to hypercapnia, while the PCr and Pi signals show some fluctuations. The first two hours under hypercapnic conditions are displayed in figure 19 B. The signal intensity of PCr is diminished after switching to hypercapnia but increases again over time. The acquisition of each spectrum takes five minutes. As shown in figure 19 C the PCr signal intensity decreases after switching back to normocapnia but also increases again after one hour. All stacked spectra are exemplarily shown for fish 3.

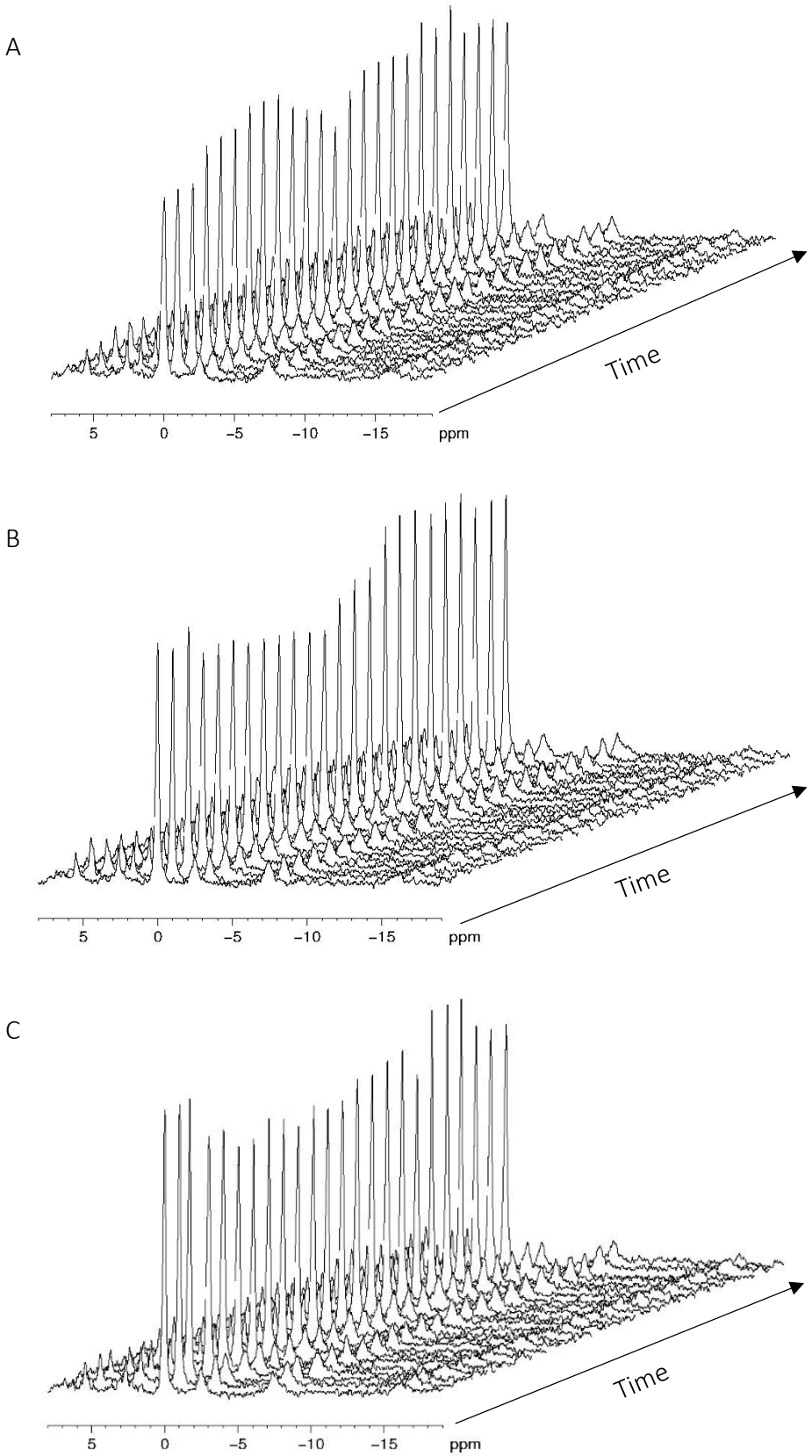

Figure 19: Stacked ^{31}P-NMR spectra of A: two hours of control conditions before switching to hypercapnia. B: the first two hours of hypercapnic conditions and C: the recovery time under normocapnic conditions after hypercapnia. The stacked spectra show the fluctuations in the signal intensity of the phosphometabolites. The acquisition of every spectrum takes five minutes. The displayed spectra were acquired in experiments with Fish 3.

3.2 Energy values

Fish 1 was showing a much higher Pi/PCr ratio during the whole experiment than the other three fish (fig. 20 A). The values for fish 1 in hypercapnic conditions are significantly higher than the values in control conditions. This is not the case for any of the other three fish (fig. 20 B-D). The Pi/PCr ratio of all four fish is displayed in figure 20 A-D. The energy values stay relatively stable during the complete time of the experiment for fish 2, 3 and 4 (fig. 20 B-D). The values of Pi/PCr ratio are in an expected range (0.05 - 0.6 ru) when compared to Kushmerick et al. (1992), Burgard (2004) and Bock et al. (2019). A relation of the Pi/PCr ratio of all four fish is shown in figure 20 E.

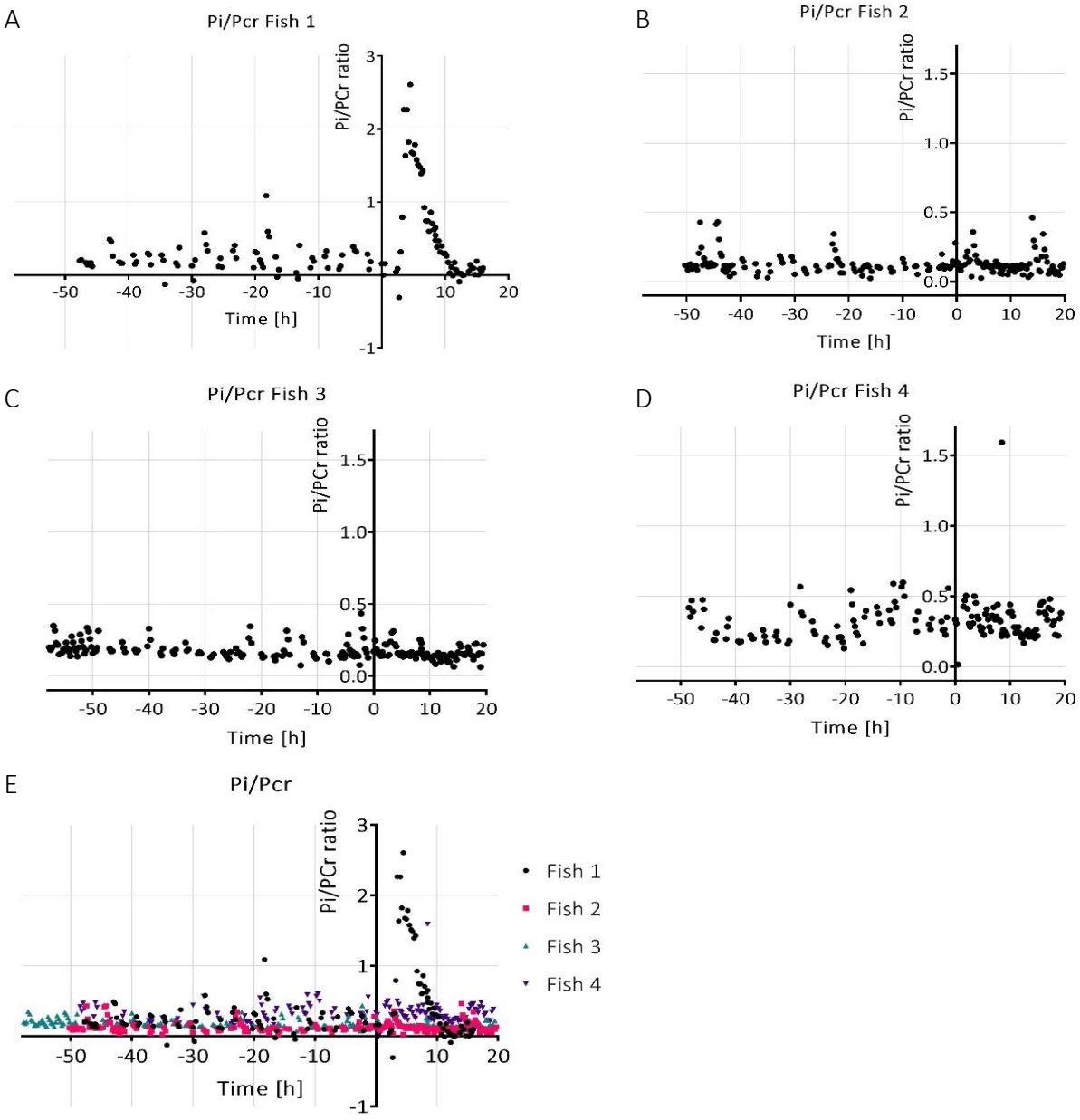

Figure 20:The energy values of every fish indicated by the Pi/PCr ratio, given in relative units [ru], and displayed in A-D. A comparison of all fish is shown in E. Time 0 is 3 hours before switching to hypercapnia.

3.3 pH_i regulation

Diagrams for all fish start with a three hour control before switching to hypercapnia, then four hours of hypercapnic conditions and then two hours of normocapnic conditions, except for fish 1 where only one hour of normocapnia could be performed. Every datapoint is 15 minutes apart from the following and represents the mean value of three ^{31}P-NMR spectroscopy measurements.

3.3.1 Fish 1

The mean pH_i of fish 1 during control is 7.46 ± 0.08 and decreases during hypercapnia by 0.6 pH units to a minimum of 6.87 ± 0.02. The mean pH_i during hypercapnia is 7.18 ± 0.08. After the hypercapnic treatment fish 1 shows an overshooting pH_i of the mean normocapnic value of 0.13 pH units to a pH_i of 7.59 ± 0.24 compared to the mean control and a maximum overshoot of 0.3 pH units (fig. 21). The pH_i as well as the pH_w were much lower for fish 1 compared to fish 2, 3 and 4. Nevertheless fish 1 survived and was still alive five weeks after the experiment. However, the energy values as well as the pH_i and pH_w of fish 1 indicate an altered experimental setup which is why fish 1 will not be taken into account for further statistical tests and will be discussed on its own. All figures showing mean values of all fish, show mean values of fish 2;3 and 4. Stacked spectra of fish 1 can be seen in the appendix (fig. 32-35).

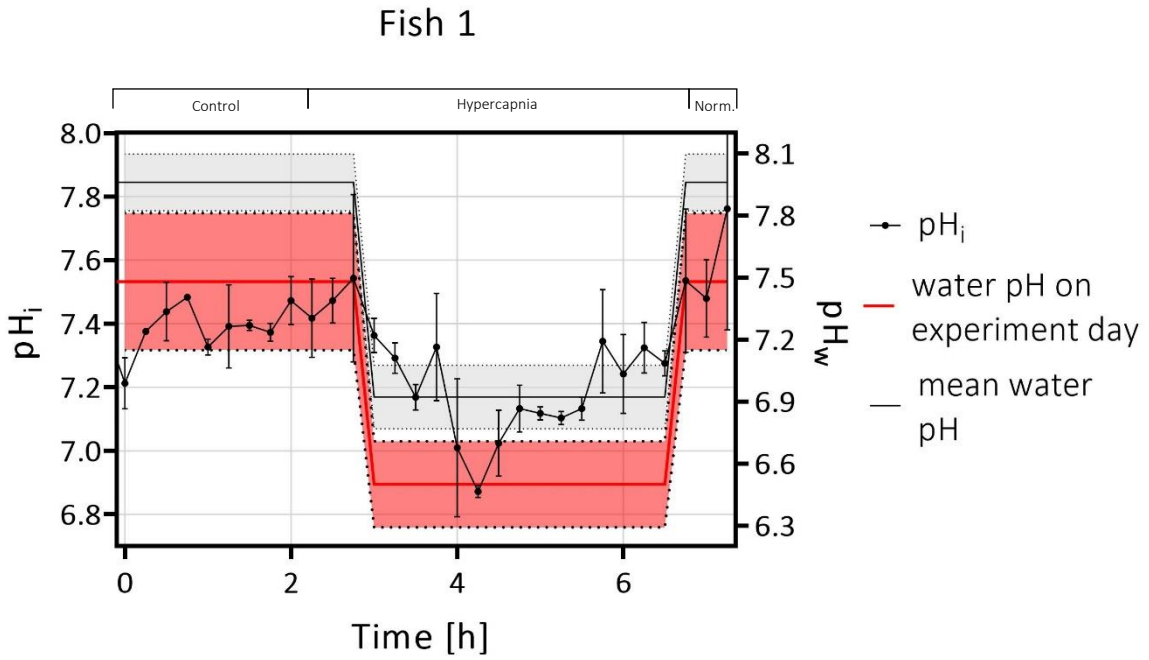

Figure 21: pH_i and pH_w of fish 1 during the experiment. Since pH_w was especially low on this experiment day it is plotted separately (red line).

3.3.2 Fish 2

The pH_i of fish 2 decreases from a mean of 7.47 ± 0.03 under control to a minimum of 7.30 ± 0.03 right after switching to hypercapnia (fig. 22). The mean pH_i during hypercapnic conditions is 7.37 ± 0.03. After switching back to normocapnia the pH_i decreases again by 0.07 pH units. The pH_i rises throughout normocapnia but the mean value for the two hours after the CO_2 treatment is just 0.01 pH units higher than under hypercapnia. There is no overshoot during normocapnia in fish 2.

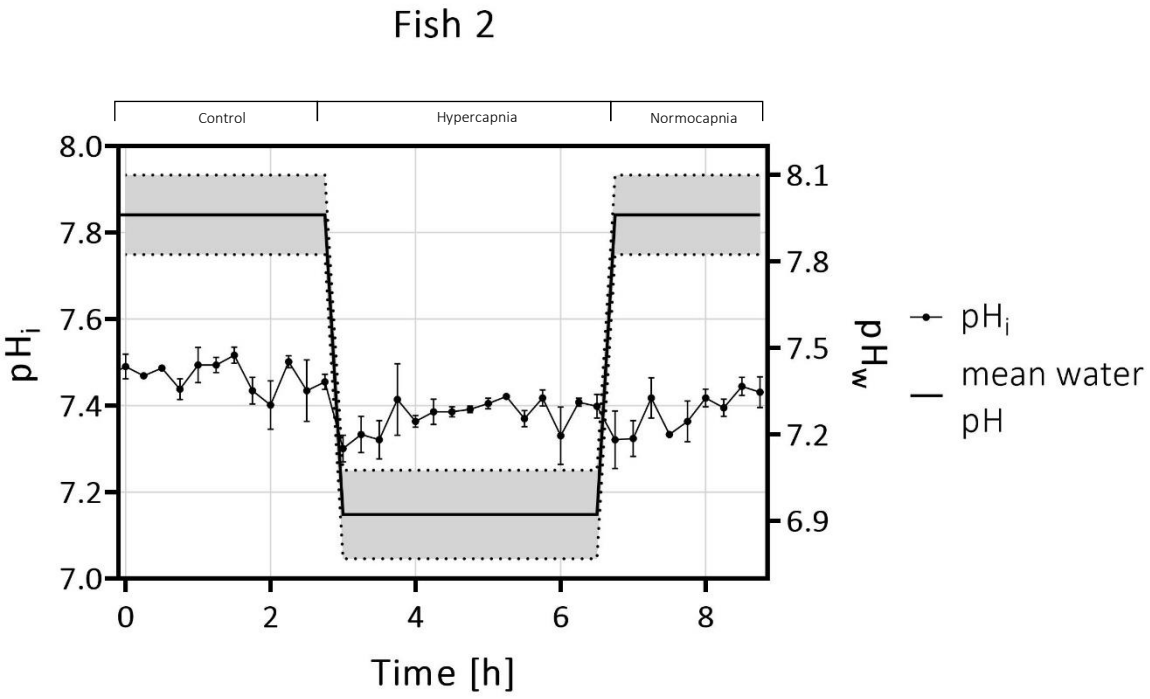

Figure 22: pH_i and pHw of fish 2 during the experiment.

3.3.3 Fish 3

Fish 3 is very stable throughout the whole experiment and only shows a decreased pH_i right after switching from control to hypercapnia (fig. 23). The pH_i decreases by 0.1 pH units from a mean of 7.47 ± 0.01 during control to 7.37 ± 0.05 under hypercapnia. But the fish can restore its pH_i quickly and the mean pH_i value during hypercapnia is 7.42 ± 0.02. The pH_i recovery is not affected by the switch back to normocapnia. The mean pH_i in the last two hours of the experiment (during normocapnia) is 7.46 ± 0.01.

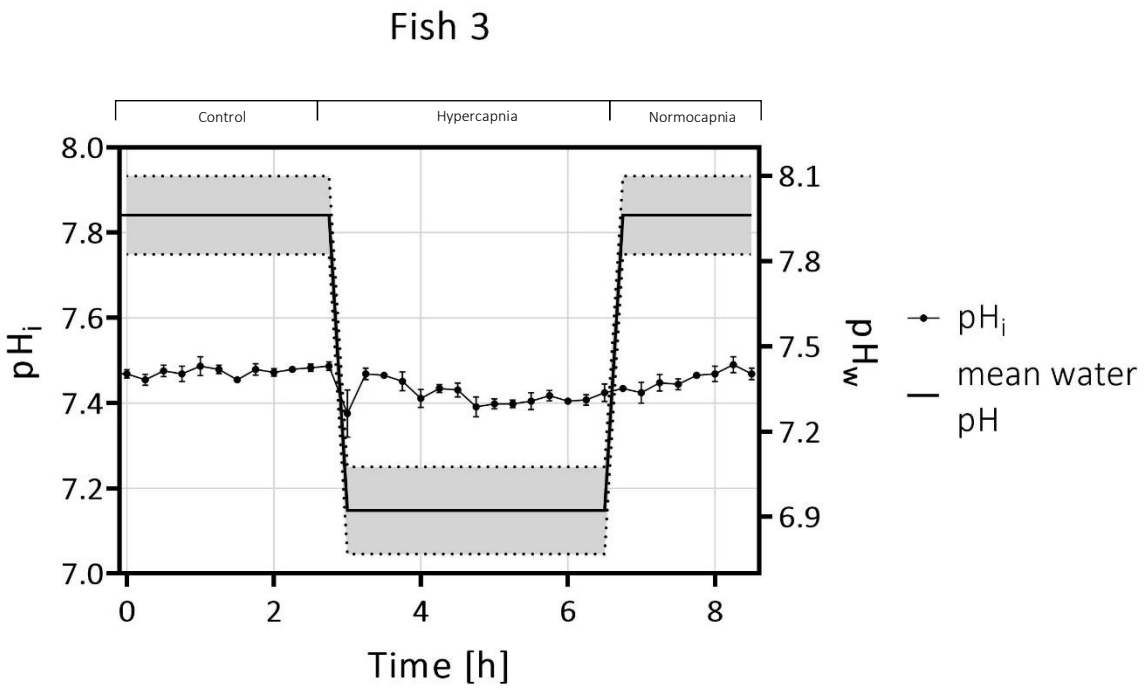

Figure 23:pH_i and pH_w of fish 3 during the experiment.

3.3.4 Fish 4

Fish 4 has a rather stable pH_i during control and a very instable pH_i during hypercapnia (fig. 24). The mean pH_i during control is 7.45 ± 0.02 and during hypercapnia 7.39 ± 0.02. The minimum pH_i during hypercapnia is 7.28 ± 0.02. During normocapnia the mean pH_i is 7.43 ± 0.01. Three

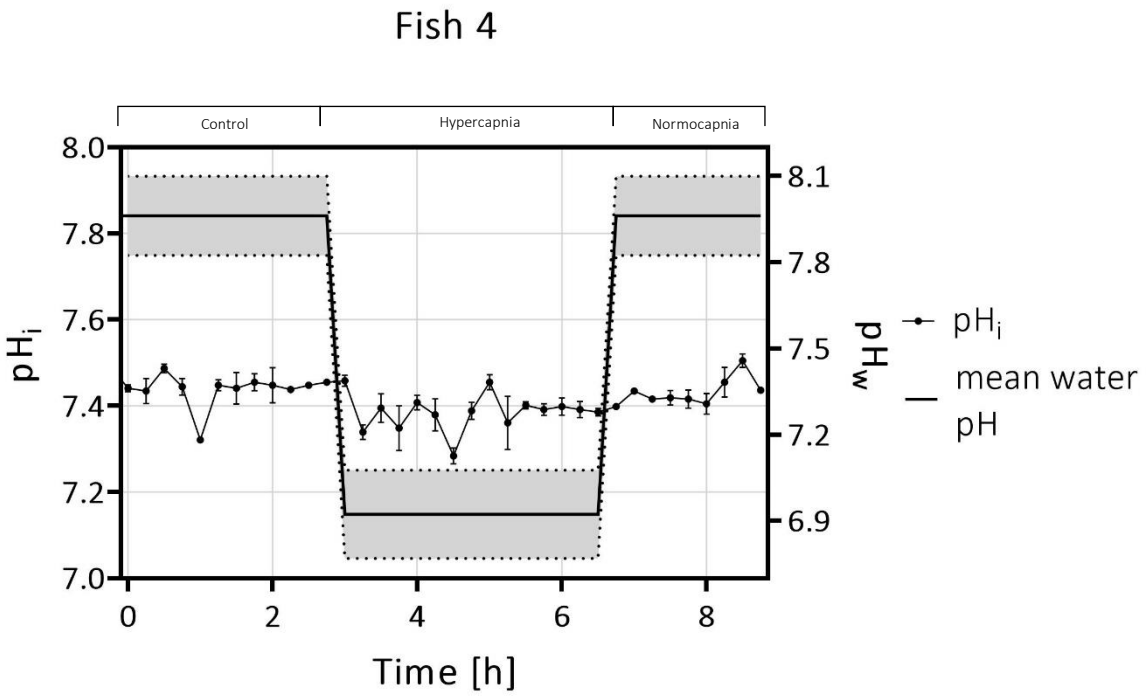

Figure 24: pH_i and pH_w of fish 4 during the experiment.

hours after switching to hypercapnia the pH_i is again stable and also does not drop again after switching back to normocapnia. Fish 4 shows a slight overshoot which is regulated again quickly.

3.3.5 Mean

When looking at the mean values of all fish in figure 25 the pH_i during control is 7.45 and it decreases during hypercapnia to a minimum of 7.37 and a mean value of 7.39. In the normocapnic treatment the mean pH_i of all fish is 7.42. As shown in figure 26 the pH_i values during hypercapnia differ significantly ($p<0.0001$) from the pH_i values during control and normocapnia.

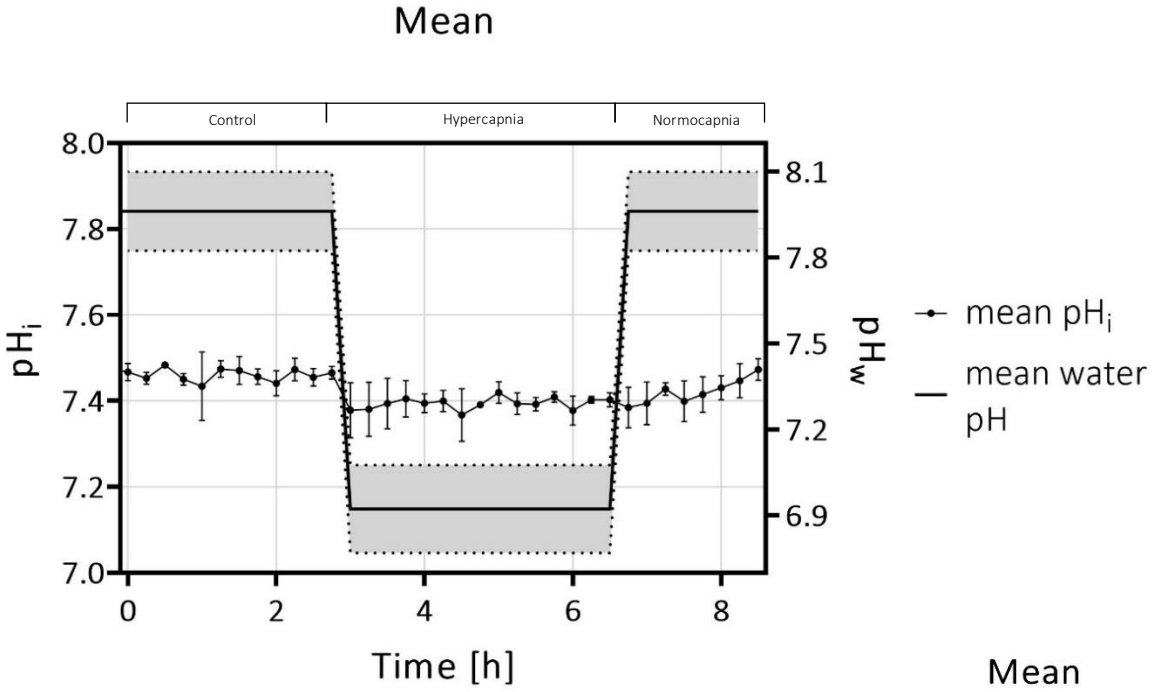

Figure 25: pH_w and a mean pH_i of fish 2, 3 and 4 during the experiment.

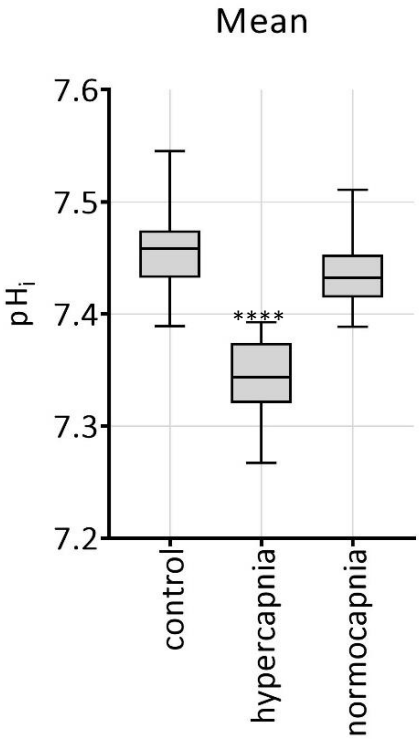

Figure 26: Boxplots of all datapoints in the three different treatments with a significant difference (p-value < 0.001) of the datapoints during hypercapnia compared to the control and normocapnic datapoints.

3.4 *In vivo* CEST measurements

The results of the CEST measurement also show a higher CEST effect during hypercapnia (fig. 27 A-C). The CEST effect is depending on various parameters such as temperature, solute proton concentration and pH. The CO_2 concentration, and therefore the water pH, is the only parameter that has been deliberately changed. Therefore, the higher CEST effect indicates an altered pH_i or a changed solute proton concentration. Figure 27 A shows the percentage change of the CEST effect over time during the control and hypercapnia. The CEST effect has been evaluated for a chemical shift of 1 ppm as well as 2.8 ppm. Figure 27 B and C show the mean CEST effect values for a chemical shift of 1 ppm (fig. 27 B) and 2.8 ppm (fig. 27 C).

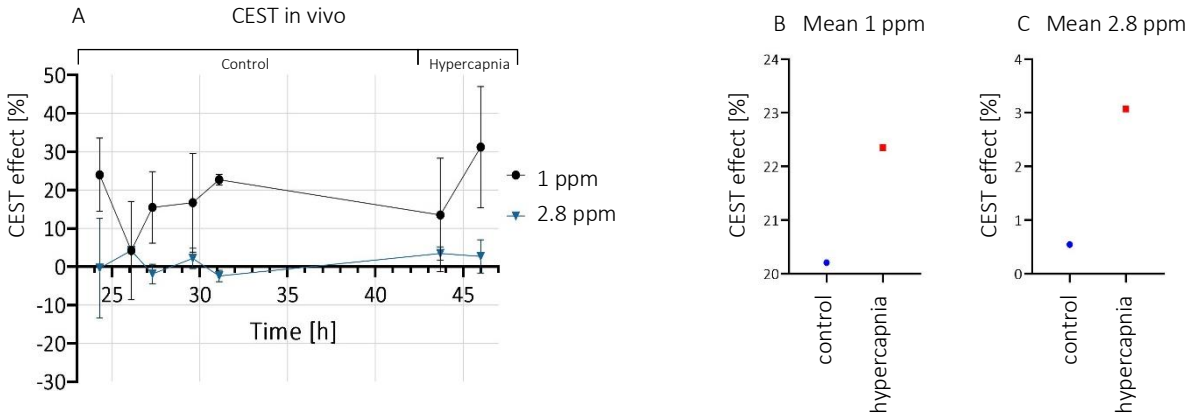

Figure 27: A: The changing CEST effect in vivo*, over time, evaluated for 1 ppm and 2.8 ppm. Every datapoint represents the mean value of three CEST measurements. The CEST results show a higher effect during hypercapnia for a chemical shit of 1 ppm as well as for 2.8 ppm. B: Mean values for the control (blue) as well as the hypercapnic (red) treatment evaluated for 1 ppm and in C: 2.8 ppm. Both graphs show a higher CEST effect during hypercapnia than during the control.*

4 Discussion

The aim of this study was the direct observation of hypercapnia induced changes in the brain of *B. saida* under OA. The energy values as well as the pH_i changes under hypercapnia were investigated with ^{31}P-NMR spectroscopy and pH_i results were verified with CEST measurements.

4.1 Water chemistry

Water parameters were tested regularly and the water was exchanged once a week but nevertheless there were fluctuations in the pH of 1 pH unit in H2 and 1.38 pH units in H1. Figure 30 gives an overview of these fluctuations. During the experiments with fish 2, 3 and 4 pH_w was close to the striven pH_w of 8 in H1 and 7 in H2. Figure 30 also shows how low pH_w was on the day of the experiment with fish 1 and confirms the decision to discuss fish 1 separately in 4.4.

pCO_2 was stable throughout the whole time of the experiment (fig. 31). Therefore, the fluctuations in pH could not be due to any fluctuations in pCO_2. A possible explanation would be that the total alkalinity (TA) was higher than expected. Measured TA was in fact higher than calculated TA . Kim et al. (2006), Kim & Lee (2009) and Kawahata et al. (2019) proposed that dissolved organic matter or organic acid, such as uric acid, can have an influence on seawater alkalinity and enhances acidification. On the other hand, those studies deal with phytoplankton and bacteria. Also fish do not excrete uric acid but ammonia and urea (Randall & Wright 1987). Still, higher alkalinity is the best explanation for the decreased pH_w.

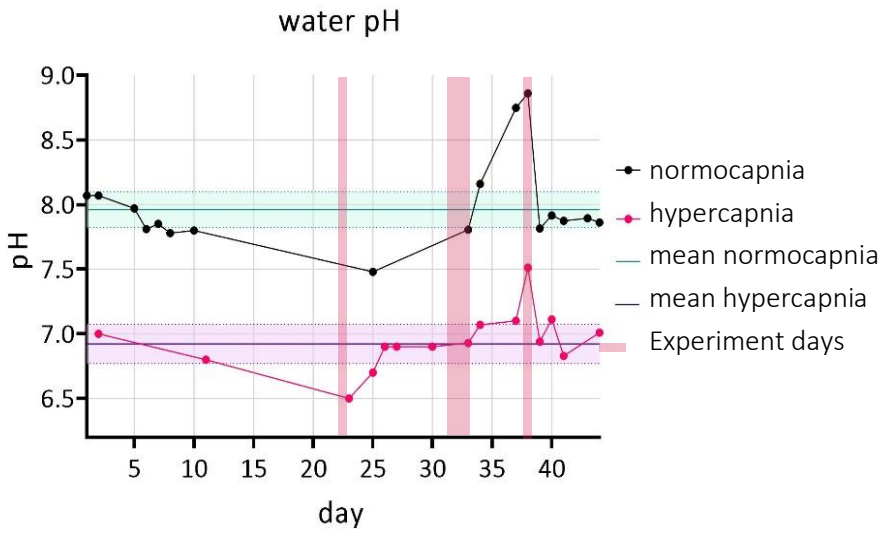

Figure 28: water pH of both H1 and H2 during the whole time of the experiment. Areas underlaid in red are actual experiment days were ^{31}P-NMR scans on B. saida *were performed.*

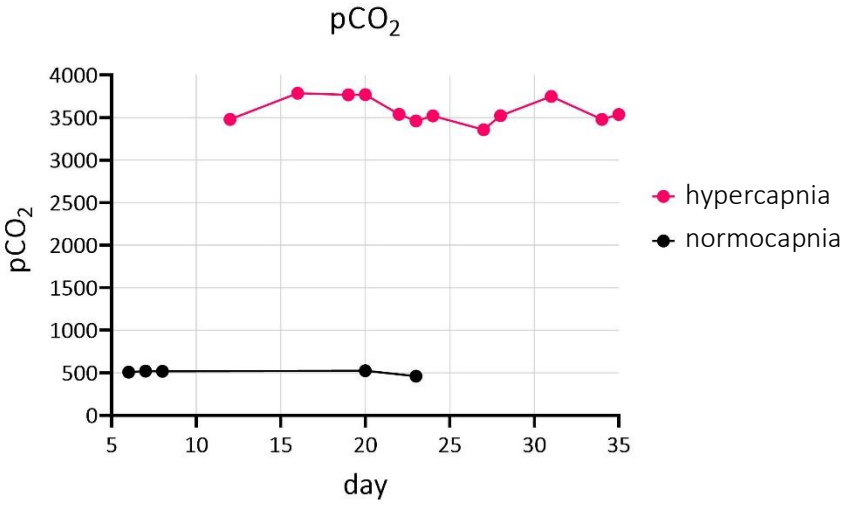

Figure 29: pCO_2 of both the normocapnic water reservoir and the hypercapnic water reservoir during the whole time of the experiment. The striven pCO_2 values for the normocapnic tank was 500 ppm and for the hypercapnic tank 3500 ppm.

4.2 pH_i regulation

Many studies investigated the importance of pH_i regulation in the brain (Chesler & Kaila 1992, Chesler 2003, Chung et al. 2014). Larsen et al. (1997) stated that the pH_i status is better regulated and more rapidly restored than pH_e. A mean pH_i of 7.45 ± 0.04 was observed under control conditions in all experimental animals over time. This is very well in the physiological range when looking at other studies on the big skate *Raja ocellate* (Mitchill, 1815) (Wood et al. 1990), on the Antarctic Black rockcod *Notothenia coriiceps* (Richardson, 1844) (Schmidt 2012), on the Antarctic eelpout *Pachycara brachycephalum* (Pappenheim, 1912) and the temperate eelpout *Zoarces viviparus* (Linnaeus, 1758) (Van Dijk et al. 1999, Mark et al. 2002). The velocity of pH regulation during hypercapnia is tissue- and species-specific (Wood et al. 1990, Larsen et al. 1997, Bock et al. 2001, Burgard 2004, Baker & Brauner 2012, Schmidt 2012, Regan et al. 2016, Wermter et al. 2018). However, in marine fish pH changes are compensated relatively fast because of the high ion concentration in the seawater and hence the amount of ions available for acid-base regulation and ionic exchange across the gills (Perry 1982, Heisler 1986). The pH_i is lowest within the first two hours after switching to hypercapnia. Afterwards, it is increasing again, until it reaches control values. The decline in pH_i starts immediately when switching to hypercapnia. The pH_i value during hypercapnia is significantly lower than the control values ($p<0.0001$). Many studies state that pH_i regulation is only completed after 24 hours (Heisler 1978, Toews et al. 1983, Wood et al. 1990, Schmidt 2012, Schmidt et al. 2014). Since hypercapnia treatment only lasted four hours in this study and after two hours pH_i values settled near control values, these results cannot be supported. After four hours pH_i correction is completed. This leads to the conclusion that a pCO_2 concentration of 3500 ppm does not pose a major threat to *B. saida*.

Burgard (2004) observed a pH_i drop under hypercapnic conditions (10 000 ppm) of 0.05 pH units in the muscle tissue of *P. brachycephalum*, using ^{31}P-NMR spectroscopy. Wood et al. (1990) performed a study on *R. ocellate* using the DMO technique (5,5-dimethyl-2,4-oxazolidinedione) technique by Waddell and Butler (1959). They observed a brain pH_i of 0.3 units lower during hypercapnia (pCO_2 = 7.5 Torr) than under control conditions. The results of Wermter et al. (2018) in a previous study on the impact of OA on *B. saida* indicate a drop in the brain pH_i of 0.2 pH units during hypercapnia (pCO_2 = 3 300 ppm), using CEST. The results of the recent study show a maximum decrease in pH_i of 0.17 in fish 2 and fish 4 and a mean decrease of 0.05 ± 0.02 in Fish 2,3 and 4 and therefore support the findings of the above-mentioned

studies. Fish 1 shows a maximum decrease of 0.9 units in the brain pH_i and is, as previously mentioned, discussed in 4.4.

4.2.1 *in vivo* CEST measurements

The results for the CEST measurements match those of Wermter et al. (2018) with an increase by 2.1% (1 ppm) and 2.5% (2.8 ppm) in the CEST effect during hypercapnia. Therefore, it can be concluded that the calculated pH by the measured CEST effect reflects the pH measured with ^{31}P-NMR spectroscopy. The evaluation for a chemical shift of 2.8 ppm displays the TauCEST effect. However, it is not yet clear which metabolite is responsible for a chemical shift of 1 ppm at low temperatures. Wermter et al. (2018) first detected a high CEST effect at low temperatures for a chemical shift of 1 ppm. The *in vitro* experiments were designed to find out which metabolite is responsible for this high CEST effect which is why phantoms were designed with BSA and TMAO, as these metabolites were not tested in the *in vitro* study of Wermter et al. (2018). BSA did not show any CEST effect higher than 6 % which is a lot less then what was found for δ at 1 ppm in the study by Wermter et al. (2018). Lee et al. (2016) investigated the CEST effect for BSA at 37°C and concluded that BSA absorbs at 2.8 ppm not 1 ppm. There is no literature about the CEST effect on TMAO. As observed in the *in vitro* experiments the CEST effect is very prominent for TMAO, but at higher temperatures than in the *in vivo* experiments. Therefore, it is very unlikely that either TMAO or BSA are responsible for the *in vivo* CEST effect of δ at 1 ppm at 1°C.

4.2.2 Active ion transport as part of pH regulation

The initial drop in intracellular pH and its increase with time indicates active acid-base regulation. pH regulation is accomplished by active mechanisms like transporters, ion channels and passive mechanisms. Fish ion homeostasis is mainly achieved by the ion transporter Na^+/K^+ ATPase as well as other active ion transporters such as H^+ ATPase and Ca^{2+} ATPase (Lin and Randall 1991, Flik and Verbost 1993). These ion transporters are ATP, hence energy dependent. The Na^+/K^+ ATPase alone uses 10% of the total ATP turnover (Gibbs and Somero, 1990). pH regulating ions are, amongst others, sodium (Na^+), hydrogen (H^+), chloride (Cl^-) and bicarbonate (HCO_3^-). Acid-base regulation seems to be more dependent on Cl^- and HCO_3^- rather than Na^+ or H^+ (Toews et al. 1983, Larsen et al. 1997). It is stated that the HCO_3^- uptake is primarily responsible for the pH_i regulation, namely the Cl^-/ HCO_3^- exchanger in the gills (Heisler 1978, Toews et al. 1983, Wood et al. 1990, Larsen et al. 1997). Baker & Brauner (2012) even

stated in a study on the white sturgeon (*Acipenser transmontanus*; Richardson, 1836) that a decrease in HCO_3^- during elevated pCO_2 may be responsible for the mortality of the fish. The accumulated HCO_3^- is gained from the environmental seawater, as Toews et al. (1983) could show in an experiment on the European conger *Conger conger* (Linnaeus, 1758). The HCO_3^- concentration in the surrounding water decreases during hypercapnia and increases in the extracellular space. In the first half an hour HCO_3^- is transferred from the intracellular to the extracellular space in the fish, but is regained afterwards from the environment (Toews et al. 1983). HCO_3^- uptake is postulated to slow down after four hours of hypercapnia (Toews et al. 1983, Milligan & Wood 1986, Wood et al. 1990). However, the meaning of these findings is conflicting. Wood et al. (1990) observed a slowed down HCO_3^- uptake and pH_i that settled at 70% of the control value, whereas Milligan & Wood (1986) showed that pH_i adjustment is fully restored after four hours of hypercapnia. Since the hypercapnic treatment in this experiment only lasted four hours, no further course can be discussed, but the results of the pH_i values indicate that after two hours pH_i settled near control values. With the recent experimental design, it was only possible to draw conclusions on the short-term, acute acclimation of *B. saida* on OA.

Fish 1, 3 and 4 show a slight overshoot of pH_i values during the recovery in normocapnia compared to the control. This phenomenon was also observed by Milligan & Wood (1986) and Burgard (2004). When pH_i is fully restored it is close to control values. There is no significant difference between pH_i during control and during the recovery in normocapnia. It is stated that the HCO_3^- concentration is responsible for this pH_i overshoot during recovery from hypercapnia (Milligan & Wood 1986).

4.2.3 Behavioural changes resulting from pH changes

As previously discussed, the main regulating ion during hypercapnia is HCO_3^-. A rising intracellular HCO_3^- concentration interferes with the $GABA_AR$ leading to a depolarization in brain cells (Regan et al. 2016). An inversion of the $GABA_AR$ could result in a shifted usage of the brain hemispheres which results in a shifted laterality (Schmidt et al. 2017). Schmidt et al. (2017) found an effect of CO_2 on the laterality of *B. saida*, which was shifted to the right during hypercapnia. Changed laterality can be a stress indicator as the left hemisphere is responsible for routine behaviour and the right hemisphere is responsible for escape and emergency

responses (Rogers 2010). Animals using primarily their right hemisphere are postulated to be stressed animals (Rogers 2010). A further stress response is discussed in paragraph 4.3.

4.3 Energy-dependent stress response

Acid-base regulation is an energy-dependent process (Riebesell et al. 2010, Maus et al. 2018). When an organism is exposed to increased pCO_2 and pH_w values, maintaining homeostasis is costly and puts the animal in a stressful situation (Claiborne et al. 2002, Popova et al. 2016). Maintaining pH_i and pH_e is costlier during hypercapnia than during normocapnia and thereby affects the whole organism energy budget (Michael et al. 2016). The Pi/PCr ratio gives a hint on the usage of energy compounds within the cell (Burgard 2004). At the beginning of hypercapnic treatment during this experiment, the PCr signal in the brain decreased, indicating reduced energy reserves in the cell to maintain ATP concentration. The Pi signal increases, indicating intracellular acidification (Bock et al. 2002). But after a maximum of 15 minutes, the PCr signal increased as well, which is why the ratio of both phosphometabolites remained largely unaffected. These results, however, are surprising as an increase of inorganic phosphate is usually accompanied by a reduction in the PCr or ATP (Kushmerick et al. 1992). Only the signal intensity of Pi increases during hypercapnia, but still not affecting the Pi/PCr or Pi/γ-ATP ratio.

Even though acid-base regulation is an energy-dependant process, the time course of Pi/PCr ratio did not show any differences between hypercapnic and normocapnic treatment (except for fish 1, fig. 20 A). There were also no differences in PCr/γ-ATP ratio during hypercapnia and normocapnia (except for fish 1, data not shown) as well as Pi/γ-ATP ratio (data not shown). These results match those of Burgard (2004) and Schmidt (2012) who also found no difference in Pi/PCr ratio as well as PCr/γ-ATP (Burgard 2004), despite a significant drop in pH_i during hypercapnia. The energy status of the brain of the animals in this study can only be discussed on the basis of the Pi/PCr, PCr/γ-ATP and Pi/γ-ATP ratio, because ^{31}P-NMR spectroscopy failed to continuously detect a β-ATP signal. The same problem was present in a study by Schmidt (2012). Since the Pi signal intensity increased during hypercapnia and the PCr as well as the ATP signals remained the same throughout control and hypercapnia, phosphometabolites had to be generated from another tissue. In fish 3 PCr signal not only remained the same but even increased during hypercapnia. A possible explanation for this would be movement of the fish and hence, detection of a different tissue. Nevertheless, acid-base regulation is an energy-dependant process and the used energy has to be restored somehow. A possible explanation

for these findings is the temporal energy buffering capacity of creatine phosphokinase (Wallimann et al. 1992). Tappan (1971) found a leakage in creatine phosphate in the muscle of the guinea pig into the blood during hypercapnia. Moreover, Watanabe et al. (2016) also found changes in the PCr signal intensity in the brain of mice during hypercapnia without changes in ADP or ATP concentration and pH_i calculations were performed using the creatine phosphokinase equilibrium. There remains the question of the source of the increased Pi signal intensity. Hayder (1972) found a decreased signal intensity of Pi in the erythrocytes of guinea pigs during the first six hours of hypercapnia. The increased amount of Pi in the brain could thus originate from Pi of the erythrocytes.

4.4 Fish 1

Fish 1 was accidently exposed to a much lower pH_w in comparison to the other experiments (see water chemistry). Therefore, the results of this experiment were not taken into account for any previously discussed statistical analysis and will be discussed separately in the following. Fish 1 is the only animal in this study that shows extremely high values for the Pi/PCr ratio as well as the PCr/γ-ATP ratio. Moreover, is the decrease in pH_i during hypercapnia extreme and very different from the other fish in this study. Fish 1 is also the only fish that shows a difference in the Pi/PCr ratio during hypercapnia compared to normocapnia. Not surprisingly the pH_i values during hypercapnia are significantly lower than during normocapnia and the control values. The values during normocapnia were 0.3 units higher during the control, but this difference was not significant. The lowest pH_i value during hypercapnia was 0.9 units below the highest value during normocapnia. The biggest difference in all other fish in hypercapnia to normocapnia was 0.17 pH units. Baker & Brauner (2012) investigated the effects of hypercapnia on white muscle tissue, liver and blood of *A. transmontanus* (15 – 90 mmHg pCO_2). It was observed that a drop in blood pH of 1.0 pH unit in *A. transmontanus* could not be compensated anymore. These results indicate that the decrease of 0.9 units in pH_i in fish 1 was near lethal values. The observed pH_i values as well as the Pi/PCr and PCr/γ-ATP ratios indicate severe physiological conditions, when compared to the literature, although the animal survived the experiment. This is another indicator for the tolerance of *B. saida*.

4.5 Comparison of CEST and *in vivo* ^{31}P-NMR spectroscopy

^{31}P-NMR spectroscopy as well as CEST measurements are non-invasive methods for intracellular pH determination. CEST MRI has a sensitivity advantage over ^{31}P-NMR

spectroscopy and enables the preservation of localized NMR measurements (Ji et al. 2017). pH has a direct effect on the chemical exchange in metabolites, which makes CEST an ideal method to observe any changes in pH *in vivo* (Kogan et al. 2013). Limitations to the CEST method are the exact determination and quantification of pH values. Any movement of objects will hamper CEST MRI, which is challenging when working with unanaesthetised and unfixed animals. One advantage of *in vivo* ^{31}P-NMR spectroscopy over CEST is the acquisition time. While the acquisition of non-localized ^{31}P-NMR spectroscopy in this study only took five minutes, the acquisition of an *in vivo* CEST MRI took 45 minutes. Therefore, any short-term changes in pH are not visible in CEST measurements, but they are in ^{31}P-NMR spectroscopy. CEST is sensitive to changes in the solute proton concentration, temperature and pH (Kogan et al. 2013, Pavuluri & McMahon 2017, Wermter et al. 2018). When temperature is stable, an increase in the solute proton concentration or a decreased pH can be responsible for the increased CEST effect.

Non-localized ^{31}P-NMR spectroscopy cannot determine the pH in an exact region as CEST measurements can, but it can provide a quantitative pH value after calibration. But also concerning the solution of exact pH values ^{31}P-NMR spectroscopy is limited. The only method, so far, that can determine the exact pH_i of an organism is the homogenate method (Pörtner et al. 1990). This method on the other hand only allows point measurements not a time course of acid-base regulation, as the organism has to be killed to conduct such measurements (Pörtner et al. 2010). Inaccuracy in evaluation of the spectrum can arise from movement of the fish, occurrence of two Pi peaks from different compartments such as muscle tissue or blood plasma, as well as the personal error. The latter can be minimised by only one person evaluating the spectra. A shift difference in Pi of 0.1 already leads to a difference in pH of 0.1 pH units. On the other hand, different Pi peaks from different compartments can also be advantageous, as one can evaluate and differentiate between different tissues (Schmidt 2012). Further discussion of the contribution of different tissues to the overall Pi peak follows. This exact determination of different peaks and the good signal to noise ratio is especially seen in a 9.4 T magnet (Schmidt 2012).

Since non-localized ^{31}P-NMR spectroscopy does not measure one explicitly selected region the question arises on how much each compartment adds to the overall Pi signal. Various studies postulated that muscle tissue (Sartoris et al. 2003), cardiac muscle (Schmidt 2012), and mitochondria (Van Waarde et al. 1990) do not add to the detected Pi signal in the brain. It is

stated that the Pi signal in these tissues is below detection limits. The only remaining tissue possibly adding to the overall Pi signal is the gill tissue. Van Waarde et al. (1990) found a detectable Pi signal of the gills with a determined pH_i of 6.98 ± 0.07 under control conditions. This is much lower than the determined pH_i of 7.45 ± 0.04 in the brain of *B. saida* in this study and thus can be excluded.

The combination of CEST and ^{31}P-NMR spectroscopy can prove the operability and accuracy of *in vivo* ^{31}P-NMR spectroscopy. In this study combining CEST and ^{31}P-NMR spectroscopy in one animal was not possible due to technical limitations. Comparing the results of both methods in the same experimental setup though, indicates that non-localized ^{31}P-NMR spectroscopy either measures primarily the brain or that the surrounding tissues do not differ significantly from the pH_i values in the brain. This hypothesis matches previously mentioned results from other studies and is supported by Schmidt (2012) and Bock et al. (2019). In both studies localized and non-localized ^{31}P-NMR spectroscopy were compared. In the recent study the combination of CEST and ^{31}P-NMR spectroscopy leads to the same conclusion that the primary compartment contributing to non-localized ^{31}P-NMR spectroscopy is the brain. Another study, combining ^{31}P-NMR spectroscopy and CEST MRI, was performed by Schüre et al. (2019) coming to the same conclusion, that CEST MRI can prove the results obtained by *in vivo* ^{31}P-NMR spectroscopy and vice versa.

The acquisition of a localized ^{31}P-NMR spectrum takes two hours and 55 minutes using a 4.7 T animal scanner (Schmidt 2012) which is even longer than it takes to acquire a CEST MRI. For this reason and the limitation in spatial resolution as well as lower sensitivity, CEST MRI is preferable to localized ^{31}P-NMR spectroscopy. Recapturing previous discussions, ^{31}P-NMR spectroscopy is the method of choice when acquiring a time-course of acid-base regulation in an organism and in combination with CEST MRI it can prove the results and can give better resolution of small pH_i changes.

4.6 Conclusions

In the present study the impact of OA on *B. saida* and its adaptation was analysed. Using non-localized ^{31}P-NMR spectroscopy it was possible to show a significant decrease of brain pH_i in *B. saida* after exposing the animal to 3500 ppm CO_2. The mean reduction in pH_i of fish 2, 3 and 4 was calculated to be 0.05 ± 0.02 and a maximum reduction was found to be 0.17. After two hours of hypercapnic treatment, pH_i started to rise again to control values and after four hours

control values were reached already. pH_i under control around 7.45, as well as under hypercapnia around 7.39, was very well comparable to literature. With the recent experimental design of four hours of hypercapnic treatment it is not possible to draw conclusions on the adaptation of *B. saida* on ocean acidification but on its short-term acclimation on acutely elevated pCO_2. CEST MRI could prove that the determined reduction in pH_i was indeed detected in the brain and that the calculated pH by the measured CEST effect reflects the pH measured with ^{31}P-NMR spectroscopy. The combination of CEST and non-localized ^{31}P-NMR spectroscopy seems like the best method combination so far to gain information about the time course of acid-base regulation and the localization of pH changes in the brain with relatively high resolution. For the present study, it can be concluded that *B. saida* can acclimatise to high pCO_2 values over a limited period of time.

However, the resolution of ^{31}P-NMR spectroscopy is not sensitive enough to detect the small changes in the path of generating ATP to regulate acid-base status within the cell. Hence, ATP generation remains questionable.

4.7 Perspectives

For further studies it would be interesting to adjust the experimental setup so that both methods (non-localized ^{31}P-NMR spectroscopy and CEST MRI) can be performed in the same organism. Wermter et al. (2018) could show that there is no learning effect in *B. saida* when exposed to hypercapnic water, so the experimental animal could be held in the chamber for several days first to acclimatise, then in hypercapnia measured with ^{31}P-NMR spectroscopy and after some time to recover again in hypercapnia measured with CEST MRI. Simultaneous measurements of both methods would be even more interesting and better to compare or to proof one another. To draw conclusions on how OA affects populations of *B. saida* it would be interesting to see how long the animal can compensate such pCO_2 values and how acid-base regulation works after not four or 24 hours of hypercapnia but after days. A similar experiment was performed by Burgard (2004) on *P. brachycephalum*. In this experiment CO_2 concentrations of 10 000 ppm pCO_2 were used that that were non-lethal for *P. brachycephalum*. However, these CO_2 concentrations are higher than anything predicted in the near future. Further research on the energy metabolism of the brain of *B. saida* is needed to understand the mechanism behind the acid-base regulation.

Bibliography

Ajiad AM, Oganin IA, Gjøsæter H (2011) Polar cod. In: Jakobsen T, Ozhigin VK, editors. The Barents Sea. Ecosystem, Resources, Management. Half a Century of Russian-Norwegian Cooperation. Trondheim: Tapir Academic Press 315-328.

Baker DW, Brauner CJ (2012) Comparative Biochemistry and Physiology, Part A Metabolic changes associated with acid–base regulation during hypercarbia in the CO_2 -tolerant chondrostean, white sturgeon (*Acipenser transmontanus*). Comp Biochem Physiol Part A 161:61–68

Biastoch A, Treude T, Rüpke LH, Riebesell U, Roth C, Burwicz EB, Park W, Latif M, Böning CW, Madec G, Wallmann K (2014) Rising Arctic Ocean temperatures cause gas hydrate destabilization and ocean acidification. Geophys Res Lett 38:1–6

Bijma J, Burhop D (2010) Ozeanversauerung - das weniger bekannte CO_2-Problem. Geogr Rundsch:16–20

Bloch F (1946) Nuclear Induction. Physical Rev 70:460-474

Boch CA, Micheli F, Alnajjar M, Monismith SG, Beers JM, Bonilla JC (2018) Local oceanographic variability influences the performance of juvenile abalone under climate change. Sci Rep:1–12

Bock C, Lurman GJ, Wittig R, Webber DM (2008) Muscle Bioenergetics of Speeding Fish: *In vivo* P-NMR Studies in a 4.7 T MR Scanner with an Integrated Swim Tunnel. Concepts Magn Reson Part B 33B:62–73

Bock C, Sartoris FJ, Pörtner H-O (2002) *In vivo* MR spectroscopy and MR imaging on non-anaesthetized marine fish: techniques and first results. Magn Reson Imaging 20:165–172

Bock C, Sartoris FJ, Wittig RM, Pörtner H-O (2001) Temperature-dependent pH regulation in stenothermal Antarctic and eurythermal temperate eelpout (Zoarcidae): An *in-vivo* NMR study. Polar Biol 24:869–874

Bock C, Wermter FC, Schalkhausser B, Blicher ME, Pörtner H-O, Lannig G, Sejr MK (2019) *In vivo* ^{31}P-MRS of muscle bioenergetics in marine invertebrates: Future ocean limits scallops ’

performance. Magn Reson Imaging 61:239–246

Bopp L, Resplandy L, Orr JC, Doney SC, Dunne JP, Gehlen M, Halloran P, Heinze C, Ilyina T (2013) Multiple stressors of ocean ecosystems in the 21st century: projections with CMIP5 models. Biogeosciences 10:6225–6245

Boscolo-Galazzo F, Crichton KA, Barker S, Pearson PN (2018) Temperature dependency of metabolic rates in the upper ocean: A positive feedback to global climate change? Glob Planet Change 170:201–212

Bozinovic F, Pörtner H-O (2015) Physiological ecology meets climate change. Ecol Evol 5:1025–1030

Bradstreet MSW (1982) Occurrence, Habitat Use, and Behavior of Seabirds, Marine Mammals, and Arctic Cod at the Pond Inlet Ice Edge. Arctic 35:28-40

Burgard C (2004) Auswirkungen erhöhter CO_2-Konzentrationen auf den Stoffwechsel von marinen Fischen

Caldeira K, Wickett ME (2003) Anthropogenic carbon and ocean pH. Nature 425:365

Caldeira K, Wickett ME (2005) Ocean model predictions of chemistry changes from carbon dioxide emissions to the atmosphere and ocean. J Geophys Res 110:1-12

Cattano C, Claudet J, Domenici P, Milazzo M (2018) Living in a high CO_2 world: a global meta-analysis shows multiple trait-mediated fish responses to ocean acidification. Ecol Monogr 88:320–335

Chambault P, Albertsen CM, Patterson TA, Hansen RG, Tervo O, Laidre KL, Heide-Jørgensen MP (2018) Sea surface temperature predicts the movements of an Arctic cetacean: The bowhead whale. Sci Rep 8:1–12

Chesler M (2003) Regulation and Modulation of pH in the Brain. Physiol Rev 83:1183–1221

Chesler M, Kaila K (1992) Modulation of pH by neuronal activity. Trends Neurosci 15:396–402

Chivers DP, McCormick, Mark I. Nilsson GE, Munday PL, Watson S, Meekan MG, Mitchell , Matthew D. Corkill KC, Ferrari MCO (2014) Impaired learning of predators and lower prey survival under elevated CO_2: a consequence of neurotransmitter interference. Glob Chang Biol 20:515–522

Christiansen JS, Schurmann H, Siikavuopio S (1996) Nonthermal Correlates of Selected Temperature in Capelin and Polar Cod - Current Lines of Research. ICES CM 1966/H:7. 13 pages

Chung W-S, Marshall NJ, Watson S-A, Munday PL, Nilsson GE (2014) Ocean acidification slows retinal function in a damselfish through interference with GABAA receptors. J Exp Biol 217:323–326

Claiborne JB, Edwards SL, Morrison-Shetlar A (2002) Acid–Base Regulation in Fishes: Cellular and Molecular Mechanisms. J Exp Zool 319:302–319

Craig P, Griffiths WB, Haldorson L, McElderry H (1982) Ecological Studies of Arctic Cod (*Boreogadus saida*) in Beaufort Sea Coastal Waters, Alaska. Can. J Fish Aquat Sci 39:395-406

Crawford R, Jorgenson J (1990) Density Distribution of Fish in the Presence of Whales at the Admiralty Inlet Landfast Ice Edge. Arctic 43:215-222

Descamps S, Aars J, Fuglei E, Kovacs KM, Lydersen C, Pavlova O, Pedersen Å, Ravolainen V, Strøm H (2017) Climate change impacts on wildlife in a High Arctic archipelago – Svalbard, Norway. Glob Chang Biol 23:490-502

Diaz RJ, Rosenberg R (1995) Marine benthic hypoxia: A review of its ecological effects and the behavioural response of benthic macrofauna. Oceanogr Mar Biol 33:245–303

Dickson A (1990) Standard potential of the reaction: AgCl(s) + 1/2 H2(g) = Ag(s) + HCl(aq), and the standard acidity constant of the ion HSO_4^- in synthetic sea water from 273.15 to 318.15 K. J Chem Thermodyn 22:113–127

Dijk PLM Van, Tesch C, Hardewig I, Pörtner H-O (1999) Physiological Disturbances at critically high temperatures: A comparison between Stenothermal antarctic and Eurythermal temperate Eelpouts (Zoarcidae). J Exp Biol 202:3611–3621

Drost HE, Carmack EC, Farrell AP (2014) Upper thermal limits of cardiac function for Arctic cod *Boreogadus saida*, a key food web fish species in the Arctic Ocean. J Fish Biol 84(6):1781–1792

Fall J, Ciannelli L, Skaret G, Johannesen E (2018) Seasonal dynamics of spatial distributions and

overlap between Northeast Arctic cod (*Gadus morhua*) and capelin (*Mallotus villosus*) in the Barents Sea. PLoS One October:1–26

Ferrari MCO, Mccormick MI, Munday PL, Meekan MG, Dixson L, Lo O, Chivers DP (2012) Effects of ocean acidification on visual risk assessment in coral reef fishes. Funct Ecol 26:553–558

Field L, Ivanova D, Bhattacharyya S, Mlaker V, Sholtz A, Decca R, Manzara A, Johnson D, Christodoulou E, Walter P, Katuri K (2018) Increasing Arctic Sea Ice Albedo Using Localized Reversible Geoengineering. Earth's Futur 6:882–901

Flik G, Verbost PM (1993) Calcium transport in Fish gills and intestine. J Exp Biol 184:17-29

Gattuso J et al. (2015) Contrasting futures for ocean and society from different anthropogenic CO_2 emissions scenarios. Oceanography 349:45–54

Gattuso J, Magnan AK, Bopp L, Cheung WWL, Duarte CM, Williamson P, Billé R, Chalastani VI, Gates RD, Irisson J-O, Middelburg JJ, Pörtner H-O, Rau GH (2018) Ocean Solutions to Address Climate Change and Its Effects on Marine Ecosystems. Front Mar Sci 5:1–18

Gibbs A, Somero GN (1990) Na +-K +-adenosine triphosphatase activities in gills of marine teleost fishes: changes with depth, size and locomotory activity level. Mar Biol 106:315-321

Gilbert D, Rabalais NN (2010) Evidence for greater oxygen decline rates in the coastal ocean than in the open ocean. Biogeosciences 7:2283–2296

Gómez1 CE, Wickes L, Deegan D, Etnoyer PJ, Cordes EE (2018) Growth and feeding of deep-sea coral Lophelia pertusa from California margin under simulated ocean acidification conditions. PeerJ 23

Graham M, Hop H (1995) Aspects of reproduction and larval biology of Arctic cod (*Boreogadus saida*). Arctic 48:130-135

Gruber N, Gruber N, Hauri C, Lachkar Z, Loher D, Frölicher TL, Plattner G (2012) Rapid Progression of Ocean Current System. Science (80-) 337:220–223

Harter BB, Elliott KH, Divoky GJ, Davoren GK (2013) Arctic cod (*Boreogadus saida*) as prey: Fish length-energetics relationships in the Beaufort sea and Hudson Bay. Arctic 66:191-196

Hassol SJ (2004) Impacts of a warming Arctic. Cambridge Univ Press

Hawkes RC, Holland GN, Moore WS, Roebuck EJ, Worthington BS (1981) Nuclear magnetic resonance (NMR) tomography of the normal heart. J Comput Assist Tomogr 5:605-612

Hayder E (1972) Studies of Calcium and inorganic Phosphorous Levels in Plasma and erythrocytes during acute and chronic Hypercapnia. Nav Submar Med Res Lab

Heisler N (1978) Bicarbonate Exchange between body compartments afterchanges of temperature in the large spottet dogfish (Scyliorhinus stellaris). Respir Physiol 33:145–160

Heisler N (1986) Acid-base regulation in fishes. Heisler N (ed) Acid-base regulation in animals Elsevier Science Publishers, Amsterdam pp 309-356

Herfkens RJ, Higgins CB, Hricak H, et al. (1983) Nuclear magnetic resonance imaging of the cardiovascular system: normal and pathological findings. A J R 147:749-759

Heuer RM, Grosell M (2016) Elevated CO_2 increases energetic cost and ion movement in the marine fish intestine. Nat Publ Gr:1–8

Heuer RM, Grosell M (2018) Physiological impacts of elevated carbon dioxide and ocean acidification on fish. Am Jounal Physiol Integr Comp Physiol 307:1016–1084

Hofmann GE, Smith JE, Johnson KS, Send U, Levin LA, Paytan A, Price NN, Peterson B, Takeshita Y, Matson PG, Crook ED, Kroeker KJ, Gambi MC, Rivest EB, Frieder CA, Yu PC, Martz TR (2011) High-Frequency Dynamics of Ocean pH: A Multi- Ecosystem Comparison. PLoS One 6

Hop H, Gjøsæter H (2013) Polar cod (*Boreogadus saida*) and capelin (*Mallotus villosus*) as key species in marine food webs of the Arctic and the Barents Sea. Mar Biol Res 9:878-894

Intergouvernmental Penal on Climate Change (IPCC) (2000) Summary for Policymakers.

Intergouvernmental Penal on Climate Change (IPCC) (2014) Climate Change 2014 Mitigation of Climate Change Working Group III Contribution to the Fifth Assessment Report of the Intergovernmental Panel on Climate Change. IPCC

Ishimatsu A, Hayashi M, Kikkawa T (2008) Fishes in high-CO2, acidified oceans. Mar Ecol Prog Ser 373:295–302

Ishimatsu A, Kikkawa T, Hayashi M, Lee K-S, Kita J (2004) Effects of CO2 on Marine Fish: Larvae and Adults Effects of CO_2 on Marine Fish : Larvae and Adults. J Oceanogr 60:731–741

Ji Y, Zhou IY, Qiu B, Sun PZ (2017) Progress toward quantitative *in vivo* chemical exchange saturation transfer (CEST) MRI. :809–824

Junium CK, Dickson AJ, Uveges BT (2018) Pertubation to the nitrogen cycle during rapid Early Eocene global warming. Nat Commun 9

Kawahata H, Fujita K, Iguchi A, Inoue M, Iwasaki S, Kuroyanagi A, Maeda A, Manaka T, Moriya K, Takagi H, Toyofuku T, Yoshimura T (2019) Perspective on the response of marine calcifiers to global warming and ocean acidification — Behavior of corals and foraminifera in a high CO_2 world "hot house." Progress in Earth and Planetary Science

Kim H, Lee K (2009) Significant contribution of dissolved organic matter to seawater alkalinity. 36:1–5

Kim H, Lee K, Choi W (2006) Contribution of phytoplankton and bacterial cells to the measured alkalinity of seawater. 51:331–338

Kogan F, Hariharan H, Reddy R (2013) Chemical Exchange Saturation Transfer (CEST) Imaging: Description of Technique and Potential Clinical Applications. Curr Radiol Rep 1:102–114

Kost GJ (1990) pH standardization for phosphorus-31 magnetic resonance heart spectroscopy at different temperatures. Magn Reson Med 14:496–506

Kroeker KJ, Kordas RL, Crim R, Hendriks IE (2013) Impacts of ocean acidification on marine organisms: quantifying sensitivities and interaction with warming. Glob Chang Biol 19:1884–1896

Kühn S, Schaafsma FL, Werven B Van, Flores H, Bergmann M (2018) Plastic ingestion by juvenile polar cod (*Boreogadus saida*) in the Arctic Ocean. Polar Biol 41:1269–1278

Kunz KL, Frickenhaus S, Hardenberg S, Johansen T, Leo E, Pörtner H-O, Schmidt M, Windisch HS, Knust R, Mark FC (2016) New encounters in Arctic waters: a comparison of metabolism and performance of polar cod (*Boreogadus saida*) and Atlantic cod (*Gadus morhua*) under ocean acidification and warming. Polar Biol 39:1137-1153

Kushmerick MJ, Moerland TS, Wiseman RW (1992) Mammalian skeletal muscle fibers distinguished by contents of phosphocreatine, ATP, and Pi. Proc Natl Acad Sci U S A 89:7521–7525

Landry JJ, Fisk AT, Yurkowski DJ, Hussey NE, Dick T, Crawford RE, Kessel ST (2018) Feeding ecology of a common benthic fish , shorthorn sculpin (*Myoxocephalus scorpius*) in the high arctic. Polar Biol 41:2091–2102

Langenbuch M, Pörtner H-O (2017) Energy budget of hepatocytes from Antarctic fish (*Pachycara brachycephalum* and *Lepidonotothen kempi*) as a function of ambient CO_2: pH-dependent limitations of cellular protein biosynthesis? J Exp Biol 206:3895–3903

Larsen BK, Pörtner H-O, Jensen FB (1997) Extra- and intracellular acid-base balance and ionic regulation in cod (*Gadus morhua*) during combined and isolated exposures to hypercapnia and copper. Mar Biol 128:337–346

Lee H, Tikunov A, Stoskopf MK, Macdonald JM (2010) Applications of chemical shift imaging to marine sciences. Mar Drugs 8:2369–2383

Lee J, Xia D, Jerschow A, Regatte RR (2016) *In vitro* study of endogenous CEST agents at 3T and 7T.

Lin H, Randall DJ (1991) Evidence for the presence of an eletrogenic proton pump on the trout gill epithelium. J Exp Biol 161:119-134

Linden A Van der, Verhoye M, Pörtner H-O, Bock C (2004) The strengths of *in vivo* magnetic resonance imaging (MRI) to study environmental adaptational physiology in fish. Magn Reson Mater Physics, Biol Med 7:236–248

Liu Y-W, Eagle RA, Aciego SM, Gilmore RE, Ries JB (2018) A coastal coccolithophore maintains pH homeostasis and switches carbon sources in response to ocean acidification. Nat Commun 9:1–12

Lonne OJ, Gulliksen B (1989) Size, Age and Diet of Polar Cod, *Boreogadus saida* (Lepechin 1773), in Ice Covered Waters. Polar Biol 9:187–191

Lurman GJ, Bock CH, Pörtner H-O (2007) An examination of the metabolic processes underpinning critical swimming in Atlantic cod (*Gadus morhua* L.) using *in vivo* ^{31}P-NMR spectroscopy. J Exp Biol 210:3749–3756

Mark FC, Bock C, Pörtner H-O, Physiol PAJ, Integr R, Physiol C (2002) Oxygen-limited thermal tolerance in Antarctic fish investigated by MRI and ^{31}P-MRS. Am Joirnal Physiol Integr

Comp Physiol 283:1254–1262

Matthaei D, Frahm J, Haase A, Hänicke W, Merboldt KD (1986) Three-dimensional FLASH MR imaging of thorax and abdomen without triggering or gating. Magn Reson Imaging 4:381-386

Maus B, Bock C, Pörtner H-O (2018) Water bicarbonate modulates the response of the shore crab Carcinus maenas to ocean acidification. J Comp Physiol B Biochem Syst Environ Physiol 188:749–764

Meinshausen M, Smith SJ, Calvin K, Daniel JS, Kainuma MLT, Lamarque J, Matsumoto K, Montzka SA, Raper SCB, Riahi K, Thomson A, Velders GJM, Vuuren DPP van (2011) The RCP greenhouse gas concentrations and their extensions from 1765 to 2300. Clim Change 109:213–241

Melzner F, Gutowska MA, Langenbuch M, Dupont S, Lucassen M, Thorndyke MC, Bleich M (2009) Physiological basis for high CO_2 tolerance in marine ectothermic animals: pre-adaptation through lifestyle and ontogeny? Biogeosciences 6:2313–2331

Michael K, Koschnick N, Pörtner HO, Lucassen M (2016) Response of branchial Na^+/K^+ ATPase to changes in ambient temperature in Atlantic cod (*Gadus morhua*) and whiting (*Merlangius merlangus*). J Comp Physiol B Biochem Syst Environ Physiol 186:461–470

Millero FJ (2010) Carbonate constants estuarine waters. Mar Freshw Res 61:139–142

Milligan CL, Wood CM (1986) Tissue intracellular acid-base status and the fate of lactate after exhaustive exercise in the rainbow trout. J Exp Biol 123:123–144

Miraux S, Massot P, Ribot EJ, Franconi J, Thiaudiere E (2008) 3D TrueFISP Imaging of Mouse Brain at 4.7 T and 9.4 T. 503:497–503

Monllor-Hurtado A, Pennino MG, Sanchez-lizaso L (2017) Shift in tuna catches due to ocean warming. PLoS One 7:1–10

Munday PL, Gagliano M, Donelson JM, Dixson DL, Thorrold SR (2011) Ocean acidification does not affect the early life history development of a tropical marine fish. Mar Ecol Prog Ser 423:211–221

Munday PL, Welch MJ, Allan BJM, Watson S-A, McMahon SJ, McCormick MI (2016) Effects of

elevated CO_2 on predator avoidance behaviour by reef fishes is not altered by experimental test water. PeerJ 4:1–18

Murray CS, Baumann H (2018) You Better Repeat It : Complex CO_2 × Temperature Effects in Atlantic Silverside Offspring Revealed by Serial Experimentation. Diversity 10:1–19

Murray CS, Malvezzi A, Gobler CJ, Baumann H (2014) Offspring sensitivity to ocean acidification changes seasonally in a coastal marine fish. Mar Ecol Prog Ser

Nilsson GE, Dixson DL, Domenici P, Mccormick MI, Sørensen C, Watson S, Munday PL (2012) Near-future carbon dioxide levels alter fish behaviour by interfering with neurotransmitter function. Nat Clim Chang 2:1–4

Oliver ECJ, Benthuysen JA, Bindoff NL, Hobday AJ, Holbrook NJ, Mundy CN, Perkins-Kirkpatrick SE (2017) The unprecedented 2015/16 Tasman Sea marine heatwave. Nat Commun 8:1–12

Oliver ECJ, Donat MG, Burrows MT, Moore PJ, Smale DA, Alexander L V., Benthuysen JA, Feng M, Gupta A Sen, Hobday AJ, Holbrook NJ, Perkins-Kirkpatrick SE, Scannell HA, Straub SC, Wernberg T (2018) Longer and more frequent marine heatwaves over the past century. Nat Commun 9:1–12

Orr JC, Fabry VJ, Aumont O, Bopp L, Doney SC, Feely RA, Gnanadesikan A, Gruber N, Ishida A, Joos F, Key RM, Lindsay K, Maier-reimer E, Matear R, Monfray P, Mouchet A, Najjar RG, Slater RD, Totterdell IJ, Weirig M, Yamanaka Y, Yool A (2005) Anthropogenic ocean acidification over the twenty-first century and its impact on calcifying organisms. Nature 437:681–686

Ou R, Yamamoto N (2016) Forebrain atlas of Japanese jack mackerel *Trachurus japonicus*. Ichthyol Res 63:405–426

Pavuluri K, McMahon MT (2017) pH Imaging Using Chemical Exchange Saturation Transfer (CEST) MRI. Isr J Chem 57:862–879

Perry AL, Low PJ, Ellis JR, Reynolds JD (2005) Climate Change and Distribution Shifts in Marine Fishes. Science 308:1912–1916

Perry SF (1982) The regulation of hypercapnic acidosis in two salmonids, the freshwater trout

(*Salmo gairdneri*) and the seawater salmon (*Oncorhynchus kisutch*). Mar Behav Physiol 9:73-79

Petrini M, Colleoni F, Kirchner N, Hughes ALC, Camerlenghi A, Rebesco M, Lucchi RG, Forte E, Colucci RR, Noormets R (2018) Interplay of grounding-line dynamics and sub-shelf melting during retreat of the Bjørnøyrenna Ice Stream. Sci Rep 8:1–9

Pierrot D, Lewis ER, Wallace DW (2006) MS Excel Program Developed for CO_2 System Calculations. ORNL/CDIAC-105a. Carbon Dioxide Information Analysis Center, Oak Ridge National Laboratory, U.S. Department of Energy, Oak Ridge, Tennessee. doi: 10.3334/CDIAC/otg.CO2SYS_XLS_CDIAC105a Pö. US Geol Surv - File Rep:1280

Popova E, Yool A, Byfield V, Cochrane K, Coward AC, Salim SS, Gasalla MA, Henson SA, Hobday AJ, Pecl GT (2016) From global to regional and back again: common climate stressors of marine ecosystems relevant for adaptation across five ocean warming hotspots. Glob Chang Biol 22:2038–2053

Pörtner H-O (2006) Climate-dependent evolution of Antarctic ectotherms: An integrative analysis. Deep Res Part II Top Stud Oceanogr 53:1071–1104

Pörtner H-O (2008) Ecosystem effects of ocean acidification in times of ocean warming: A physiologist's view. Mar Ecol Prog Ser 373:203–217

Pörtner H-O (2012) Integrating climate-related stressor effects on marine organisms: unifying principles linking molecule to ecosystem-level changes. Mar Ecol Prog Ser 470:273–290

Pörtner H-O, Bickmeyer U, Bleich M, Bock C, Brownlee C, Melzner F, Michaelidis B, Sartoris FJ, Storch D (2010) Studies of acid-base status and regulation. Guide to best practices for ocean acidification research and data reporting 137-166

Pörtner H-O, Bock C, Knust R, Lannig G, Lucassen M, Mark FC, Sartoris FJ (2008) Cod and climate in a latitudinal cline : physiological analyses of climate effects in marine fishes. Clim Res 37:253–270

Pörtner H-O, Boutilier RG, Tang Y, Toews DP (1990) Determination of intracellular pH and pCO2 after metabolic inhibition by flouride and nitrilotriacetic acid. Respir Physiol 81:255-274

Pörtner H-O, Gutowska M, Ishimatsu A, Lucassen M, Melzner F, Seibel B (2011) Effects of ocean

acidification on nektonic organisms. Ocean acidification, Chapter 8. In: ocean acidification.p 154–162

Pörtner H-O, Langenbuch M, Michaelidis B (2005) Synergistic effects of temperature extremes, hypoxia, and increases in CO_2 on marine animals: From Earth history to global change. J Geophys Res 110:1–15

Pörtner H-O, Langenbuch M, Reipschlager A (2004) Biological Impact of Elevated Ocean CO_2 Concentrations: Lessons from Animal Physiology and Earth History. J Oceanogr 60:705–718

Praetorius S, Rugenstein M, Persad G, Caldeira K (2018) Global and Arctic climate sensitivity enhanced by changes in North Pacific heat flux. Nat Commun 9:1–12

Pritchard RB, Flemming Hansen D (2019) Characterising side chains in large proteins by protonless ^{13}C-detected NMR spectroscopy. Nat Commun 10:1747–1754

Purcell E, Torrey HC, Pound RV (1946) Resonance Absorption by Nuclear Magnetic Moment in a solid. Physical Rev 69:37-38

Randall DJ, Wright PA (1987) Ammonia distribution and excretion in fish. Fish Physiol Biochem 3:107–108

Regan MD, Turko AJ, Heras J, Andersen MK, Lefevre S, Wang T, Bayley M, Brauner CJ, Huong DTT, Phuong NT, Nilsson GE (2016) Ambient CO_2, fish behaviour and altered GABAergic neurotransmission: exploring the mechanism of CO_2-altered behaviour by taking a hypercapnia dweller down to low CO_2 levels. J Exp Biol 219:109–118

Renaud P, Berge J, Varpe O, Lønne OJ, Nahrgang J, Ottesen C, Hallanger I (2012) is the poleward expansion by Atlantic cod and haddock threatening native polar cod, *Boreogadus saida*? Polar Biol 35:401-412

Riebesell U, Fabry V, Hansson L, Gattuso J (2010) Guide to best practices for ocean acidification research and data reporting.

Ripps H, Shen W (2012) Review: Taurine: A “very essential” amino acid. Mol Vis 18:2673–2686

Rogers LJ (2010) Relevance of brain and behavioural lateralization to animal welfare. Appl Anim Behav Sci 127:1–11

Rueden CT, Schindelin J, Hiner MC, DeZonia BE, Walter AE, Arena ET, Eliceiri KW (2017) ImageJ2: ImageJ for the next generation of scientific image data. BMC Bioinformatics 18:1–26

Sartoris FJ, Bock C, Serendero I, Lannig G, Pörtner H-O (2003) Temperature-dependent changes in energy metabolism, intracellular pH and blood oxygen tension in the Atlantic cod. J Fish Biol 62:1239–1253

Schild HH (1990) MRI made easy.

Schindelin J, Arganda-Carreras I, Frise E, Kaynig V, Longair M, Pietzsch T, Preibisch S, Rueden C, Saalfeld S, Schmid B, Tinevez J-Y, White DJ, Hartenstein V, Eliceiri K, Tomancak P, Cardona A (2012) Fiji: an open-source platform for biological-image analysis. Nat Methods 9:676–82

Schmidt M (2012) Investigating physiological effects of hypercapnia on the brain of Notothenia coriiceps using *in vivo* NMR spectroscopy and imaging

Schmidt M (2019) Behavioural disturbances and underlying neurophysiological mechanisms during ocean acidification and warming in *Gadus morhua* and *Boreogadus saida*

Schmidt M, Gerlach G, Leo E, Kunz KL, Swoboda S, Pörtner H, Bock C, Storch D (2017) Impact of ocean warming and acidification on the behaviour of two co-occurring gadid species, *Boreogadus saida* and *Gadus morhua*, from Svalbard. Mar Ecol Prog Ser 571:183–191

Schmidt T, Ghaffarian N, Philippot C, Seifert G, Steinhäuser C, Pape H, Blaesse P (2018) Differential regulation of chloride homeostasis and GABAergic transmission in the thalamus. Sci Rep 8:1–11

Schmidt M, Pörtner H-O, Bock C (2014) A new set-up to investigate neurophysiological effects of CO_2-induced ocean acidification on the brain of fish via MR imaging and spectroscopy. Proc. Intl. Soc. Mag. Reson. Med. 22:4661

Schüre J, Shrestha M, Breuer S, Deichmann R, Hattingen E, Wagner M, Pilatus U (2019) The pH sensitivity of APT-CEST using phosphorus spectroscopy as a reference method. NMR Biomed:1–12

Scott WB, Scott MG (1988) Atlantic fishes of Canada

Shartau RB, Baker DW, Crossley DA, Brauner CJ (2016) Preferential intracellular pH regulation:

hypotheses and perspectives. Co Biol 219:2235–2244

Siesjö BK, Folbergrová J, MacMillan V (1972) The effect of hypercapnia upon intracellular pH in the brain, evaluated by the bicarbonate-carbonic acid method and from the creatine phosphokinase equilibrium. J Neurichemistry 19:2483–2495

Sinning A, Hübner CA (2013) Minireview : pH and synaptic transmission. FEBS Lett 587:1923–1928

Tappan D (1971) Biochemistry of submarine and diving stress III. Plasma Creatine, Creatine Phosphate and Creatine Phosphokinase response to hypercapnia. Submar Med Res Laboratoy

Thillart G Van den, Körner F, Waarde A Van, Erkelens C, Lugtenburg J (1989) A Flow-Through Probe for *in vivo* ^{31}P-NMR Spectroscopy of Unanesthetized Aquatic Vertebrates at 9.4 Tesla. J Magn Reson 519:573–579

Toews DP, Holetonj GF, Heisler N (1983) Regulation of the acid-base status during environmental hypercapnia in the marine teleost fish *Conger conger*. J Exp Biol 107:9–20

Turingan R, Sloan T (2016) Thermal Resilience of Feeding Kinematics May Contribute to the Spread of Invasive Fishes in Light of Climate Change. Biology (Basel) 5:1–15

Uppström LR (1974) The boron/chlorinity ratio of deep-sea water from the Pacific Ocean. Deep Sea Res Oceanogr Abstr 21:161-162.

Verberk WCEP, Bilton DT, Calosi P, Spicer JI (2011) Oxygen supply in aquatic ectotherms: Partial pressure and solubility together explain biodiversity and size patterns. Ecology 92:1565–1572

Waarde A Van, Thillart G Van Den, Bonga SW (1990) ^{31}P-NMR Studies on Acid-Base Balance and Energy Metabolism of Acid- Exposed Fish. J Exp Biol 154:223–236

Waddell, W.J. and T. C. Butler (1959). Calculation of intracellular pH from the distribution of 5,5-dimethyl- 2,4-oxazolidine dione (DMO): application to skeletal muscle of the dog. J. Clin. Invest. 38: 720-729

Walker-Samuel S, Ramasawmy R, Torrealdea F, Rega M, Rajkumar V, Johnson SP, Richardson S, Gonçalves M, Harold G, Årstad E, Thomas DL, Pedley RB, Lythgoe MF (2017) Europe PMC

Funders Group *In vivo* imaging of glucose uptake and metabolism in tumors. Nat Med 19:1067–1072

Wallimann T, Wyss M, Brdiczka D, Nicolay K, Eppenberger HM (1992) Intracellular compartmentation, structure and function of creatine kinase isoenzymes in tissues with high and fluctuating energy demands: the 'phosphocreatine circuit' for cellular energy homeostasis. Biochem J 281:21–40

Ward KM, Aletras AH, Balaban RS (2000) A New Class of Contrast Agents for MRI Based on Proton Chemical Exchange Dependent Saturation Transfer (CEST). J Magn Reson 87:79–87

Ward KM, Balaban RS (2000) Determination of pH Using Water Protons and Chemical Exchange Dependent Saturation Transfer (CEST). Magn Reson Med 802:799–802

Watanabe T, Frahm J, Michaelis T (2016) Amide proton signals as pH indicator for *in vivo* MRS and MRI of the brain-Responses to hypercapnia and hypothermia. Neuroimage 133:390–398

Webb RK, Wodhall PB, Tisher CC, Glaubiger G, Neelon F, Robinson RR (1977) Relationship between phosphaturia and acute hypercapnia in the rat. J Clin Invest 60:829–837

Welch HE, Bergmann MA, Sieferd TD, Martin KA, Curtis MF, Crawford RE, Conover RJ, Hop H (1992) Energy flow through the marine ecosystem of the Lancaster Sound region, Arctic Canada. Arctic 45:343-357

Wermter FC, Bock C, Dreher W (2015) Investigating GluCEST and its specificity for pH mapping at low temperatures. NMR Biomed 28:1507–1517

Wermter FC, Bock C, Maus B, Pörtner H-O, Dreher W (2018) CO_2 induced pH_i changes in the brain of polar fish: a TauCEST application. NMR Biomed 31:1–12

Wilson LJ, Fulton CJ, Hogg AM, Joyce KE, Radford BTM, Fraser CI (2016) Climate-driven changes to ocean circulation and their inferred impacts on marine dispersal patterns. Glob Ecol Biogeogr 25:923–939

Wood CM, Turner JD, Munger RS, Graham MS (1990) Control of ventilation in the hypercapnic skate Raja ocellata: II. Cerebrospinal fluid and intracellular pH in the brain and other

tissues. Respir Physiol 80:279–298

Zhuang X, Yang C, Fevolden SE and Cheng C (2012) Protein genes in repetitive sequence—antifreeze glycoproteins in Atlantic cod genome. BMC Genomics 13:293-301

Zijl PCM Van, Yadav NN (2011) Chemical Exchange Saturation Transfer (CEST): What is in a Name and What isn't? Magn Reson Med 65:927–948

Zittier ZMC, Bock C, Sukhotin AA, Häfker NS, Pörtner H-O (2018) Impact of ocean acidification on thermal tolerance and acid–base regulation of *Mytilus edulis* from the White Sea. Polar Biol 41:2261–2273

http://www.ipcc.ch/ipccreports/sres/emission/index.php?idp=94 , 03.11.2018

https://www.co2.earth/daily-co2 , 02.08.2019

Appendix

Table 3:Scan properties of all performed NMR scans in this study (^{31}P-NMR spectroscopy, in vitro *CEST and* in vivo *CEST measurements).*

Scan properties	^{31}P-NMR spectroscopy	*In vitro* CEST	*In vivo* CEST
method	^{31}P-Singlepulse	Pre-saturated FISP	Pre-saturated FISP
FOV		30 x 30 mm^2	48 x 48 mm^2
Matrix size		64 64	
Slice thickness		2 mm	4 mm
Flip angle	65°	9°	9 °
T_R	1200 ms	3.2 ms	3 ms
T_E		1.6 ms	1.65 ms
Frequency offset		−20 000, −10 000, −5000, −2250, −2125, −2000, −1875, −1750, −1625, −1500, −1375, −1250, −1125, −1000, −875, −750, −625, −500, −375, −250, −188, −125, −62, 0, 62, 125, 188, 250, 375, 500, 625, 750, 875, 1000, 1125, 1250, 1375, 1500, 1625, 1750, 1875, 2000, 2125, 2250, 5000, 10 000 and 20 000, all in Hz	
Acquisition bandwidth	10 000 Hz		
Reference power	2.714 W		
Excitation pulse	bp32		
Pulse length	0.2 ms		
Pulse power	16.9625 W		
Averages	256	4	4

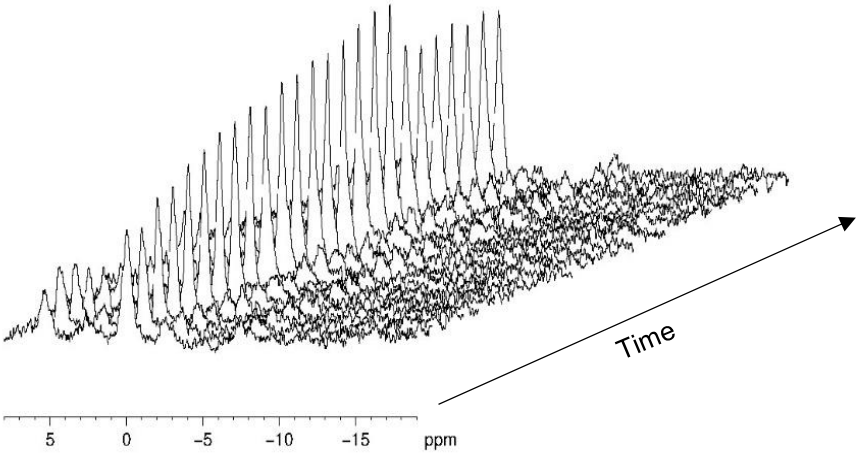

Figure 30: Stacked ^{31}P-NMR spectra of two hours of control conditions before switching to hypercapnia in the experiment in fish 1.

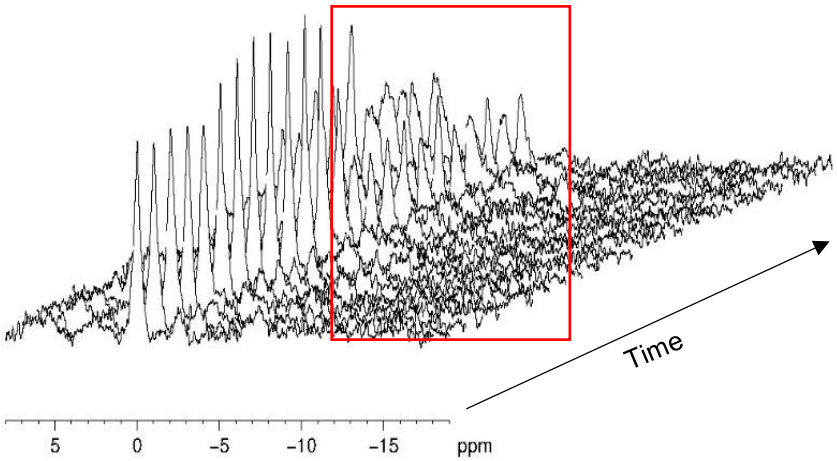

Figure 31: Stacked ^{31}P-NMR spectra of one hour of control and one hour of hypercapnia in the red box in the experiment with fish 1.

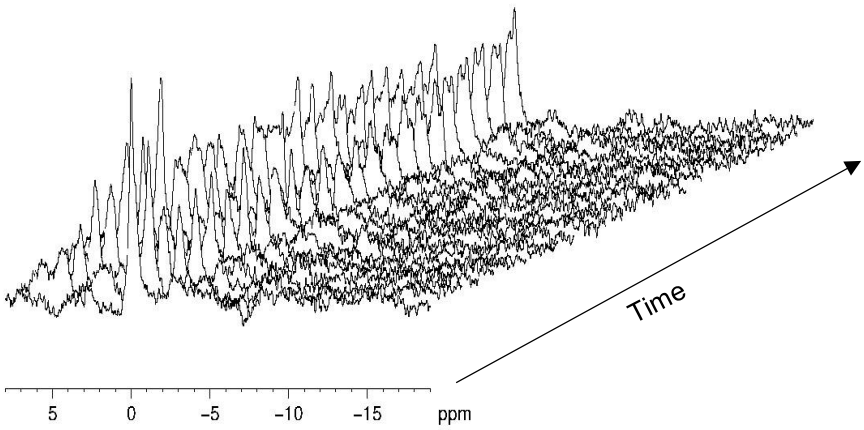

Figure 32: Stacked ^{31}P-NMR spectra of the first two hours of hypercapnic treatment in the experiment with fish 1.

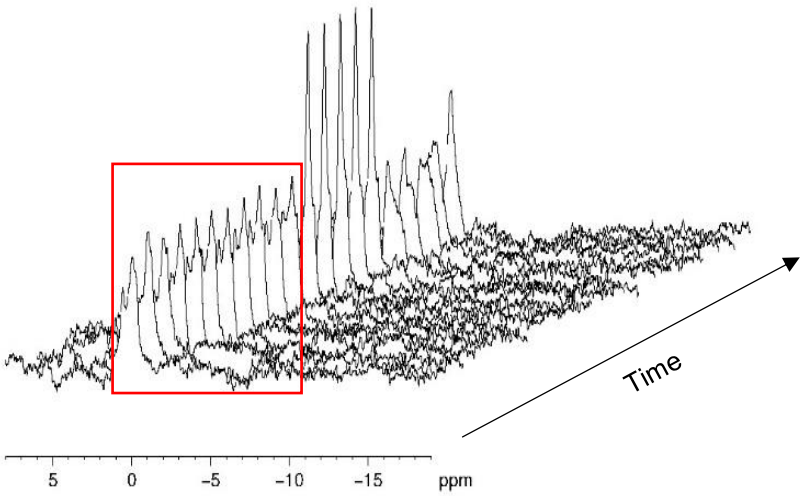

Figure 33: Stacked ^{31}P-NMR spectra of the last two hours of hypercapnic treatment in the red box and then the normocapnic treatment outside the red box for the experiment with fish 1.

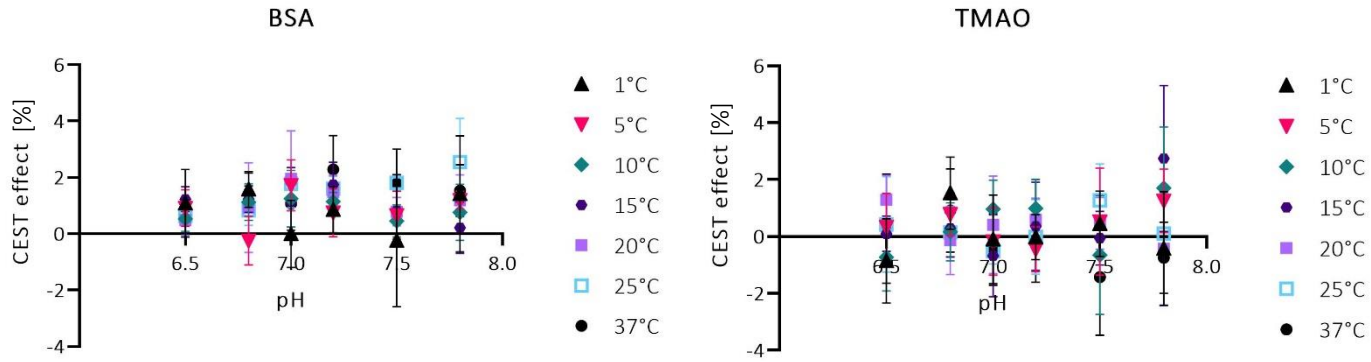

Figure 34: The CEST effect for BSA and TMAO evaluated at 2.8 ppm on a smaller scale. The CEST Effect is again higher for TMAO than for BSA.

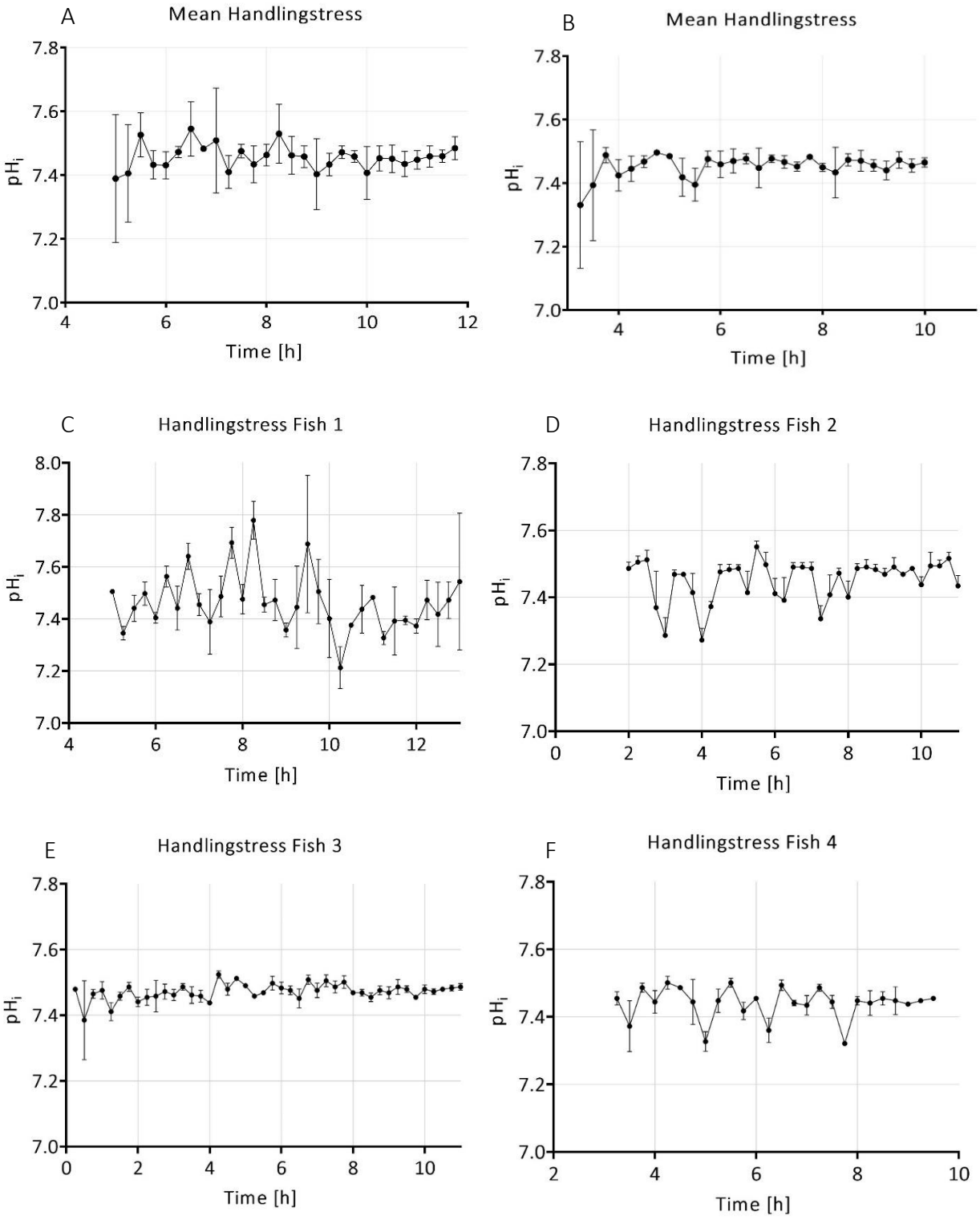

Figure 35: Shown here are the first hours after placing the experimental animal in the testing chamber. A: Mean values for fish 1, 2, 3 and 4. B: Mean value for fish 2, 3 and 4.C-F show the values for each fish alone.

Acknowledgements

I want to thank

Prof. Dr. Hans-Otto Pörtner for giving me the opportunity to work on this topic.

Dr. Christian Bock for his valuable advice and his optimism that cannot be broken.

Prof. Dr. Inna Sokolova for grading and agreeing to write an external thesis.

Bastian Maus for his help with the MRT whenever technique didn't do what I wanted it to do.

Dr. Felizitas Wermter for guidance regarding CEST, MRT and graphic presentation of the results.

Fredy Vèliz Moraleda for answering all my questions about fish handling, water chemistry and the secrets of pH measuring.

Anette Tillmann for helping me and introducing me to the laboratory as well as the whole section Integrative Ecophysiology for all the support and the welcoming atmosphere.

Jan-Phillipp Geissel for the mental and hands-on support in our cellar laboratory where one could easily forget the time and day if not loose sanity.

Especially my **family** and **friends** who supported me and always listened whenever I was nervous about the outcome or doubted what I was doing and pushed me or distracted me depending on what I needed.

Declaration

Hereby I declare that this Master's Thesis has been written by me without external support and that I did not use any other than the quoted sources and auxiliary means. All statements which are literally or analogously taken from other publications have been identified as quotations. After having handed in my Master`s Thesis, no further modifications will be conducted. This work has not been published or submitted for grading anywhere else.

_____

Clara Isabella Scheuring,

Rostock, 2nd of September 2019